Microtubule Feedback and LET-99-Dependent Control of Pulling Forces Ensure Robust Spindle Position

Helene Bouvrais, Laurent Chesneau, Sylvain Pastezeur, Danielle Fairbrass, Marie Delattre, Jacques Pécréaux

Microtubule feedback and LET-99-dependent control of pulling forces ensure robust spindle position.

Hélène Bouvrais[1,*], Laurent Chesneau[1], Sylvain Pastezeur[1], Danielle Fairbrass[1], Marie Delattre[2], and Jacques Pécréaux[1,*]

Running title:
Dual control of pulling forces

Affiliations

[1] CNRS, Univ Rennes, IGDR – UMR 6290, F-35000 Rennes, France.

[2] Univ Lyon, ENS de Lyon, Univ Claude Bernard, Laboratory of Biology and Modelling of the Cell, Lyon University, Lyon, France

Correspondence: helene.bouvrais@univ-rennes1.fr (ORCID # 0000-0003-1128-1322); jacques.pecreaux@univ-rennes1.fr (ORCID # 0000-0001-9998-4844)

ABSTRACT

During asymmetric division of *Caenorhabditis elegans* zygote, to properly distribute cell fate determinants, the mitotic spindle is asymmetrically localized by a combination of centering and cortical pulling microtubule-mediated forces, the dynamics of the latter being regulated by mitotic progression. Here we show a novel and additional regulation of these forces by spindle position itself. For that, we observed the onset of transverse spindle oscillations which reflects the burst of anaphase pulling forces. After delaying anaphase onset, we found that the position at which the spindle starts to oscillate was unchanged compared to control embryos and uncorrelated to anaphase onset. In mapping the cortical microtubule dynamics, we measured a steep increase in microtubule contact density after the posterior centrosome reached the critical position of 70% of embryo length, strongly suggesting the presence of a positional switch for spindle oscillations. Expanding a previous model based on a force-generator temporal control, we implemented this positional switch and observed that the large increase in microtubule density accounted for the pulling force burst. Thus, we propose that the spindle position influences the cortical availability of microtubules, on which the active force generators, controlled by cell cycle progression, can pull. Importantly, we found that this positional control relies on the polarity-dependent LET-99 cortical band, whose boundary could be probed by microtubules. This dual positional and temporal control well accounted for our observation that the oscillation onset position resists changes in cellular geometry and moderate variations in the active force generator number. Finally, our model suggests that spindle position at mitosis end is more sensitive to the polarity factor LET-99, which restricts the region of active force generators to a posterior-most region, than to microtubule number or force generator number/activity. Overall, we show that robustness in spindle positioning originates in cell mechanics rather than biochemical networks.

INTRODUCTION

Asymmetric cell divisions, with their differing daughter cell sizes, contents, and fates, are essential to achieve cellular diversity during development (1, 2). In the nematode *Caenorhabditis elegans*, as in many other species, during the first embryonic division, the mitotic spindle is oriented along the polarity axis and displaced out of the cell center (3, 4), where it helps position the cytokinesis cleavage furrow (5-8). Most asymmetric divisions include pulling forces from the cell cortex that are exerted on the astral microtubule plus ends, and these forces are key in positioning and orienting the mitotic spindle (3, 4, 9). In the one-cell nematode embryo, cortical forces are generated by a well-conserved trimeric complex which pulls on astral microtubules. The complex is made up of a dynein/dynactin complex, a LIN-5 protein (homolog of NuMA), and the G-protein regulators GPR-1/2, which are mammalian LGN homologs (10). In an asymmetric division, GPR-1/2 proteins reflect polarity cues (11) through their asymmetric locations at the cortex (11-13), increasing the number of *active* force generators at the embryo posterior-most side (11, 14, 15). Active force generator is defined as a complex either currently pulling from the cortex, or ready to do so upon meeting a microtubule (10, 16, 17).

In our initial "tug-of-war" physical model, we focused on the spindle oscillation and posterior displacement. We found that, along the anaphase course, an embryo-wide decrease in the force generator detachment rate from astral microtubules accounted for the oscillation build-up and die down, and for the increase in the pulling force imbalance, thus causing posterior spindle displacement (16). The suggested temporal regulation was reinforced by the proposed link between spindle displacement timing and the cell cycle (18). In our initial model, we assumed that astral microtubules were abundant at the cortex during anaphase, and that the only limiting factor was the binding/unbinding dynamics of the force generators from the microtubules. Since then, Kozlowski *et al*. proposed a model that accounted for spindle oscillation by the limited access of the astral microtubules to the cortex (19). Furthermore, some studies showed that perturbations to microtubule dynamics, while mild enough to prevent catastrophic phenotypes, resulted in an alteration to final spindle position (20, 21). These results call for a re-examining of the role of astral microtubules in spindle positioning. In addition, we recently observed that the position of the posterior centrosome at which oscillation begins, hereafter called oscillation onset position, was not synchronized with mitotic progression in the cousin species *Caenorhabditis briggsae* (13), indicating that some other mechanism(s) contribute to regulating the cortical pulling forces.

Interestingly, the same machinery controlling spindle position and rocking at anaphase also accounts for the final spindle position. Furthermore, the mechanism connecting cortical polarity cues to the forces that set the final spindle position, and how this mechanism ensures a robust positioning of the mitotic spindle remains an open question. The LET-99 DEP-domain (Disheveled, Egl-10 and Pleckstrin domain) containing protein is an important part of this mechanism (22) and acts downstream to PAR polarity proteins (23). Indeed, a band of LET-99 located at the cortex, spanning from 45% to 70% of embryo length, is devoid of force generation (24). To account for how LET-99 contributes to spindle positioning, two possible, not exclusive mechanisms were proposed. Firstly, LET-99 could relocalize all GPR-1/2

proteins found at the posterior cortex to the posterior-most crescent, increasing their concentration, and in turn creating an imbalance in the number of active force generators at the cortex (15). Posterior displacement of the spindle following LET-99 depletion, however, puts this mechanism into question (24). Secondly, LET-99 could act by inhibiting the GPR-1/2 proteins located in the 45%-70% cortical band (termed posterolateral) and thus only constraining the cortical location at which forces can be generated, a so-called spatial restriction mechanism. In this case, the higher concentration of GPR-1/2 in the embryo's posterior half (12, 13) would then be caused by another mechanism, still linked to polarity. While this second possibility is attractive, the spatial restriction mechanism is still unknown. One proposed mechanism was the contribution of the orientation of the pulled astral microtubules (25), in which LET-99 could inhibit forces oriented backward with respect to spindle displacement. This nevertheless does not account for LET-99 depletion resulting in a strong anterior shift in the final spindle position (22-24). Overall, how the LET-99 cortical band contributes to final spindle positioning remains to be understood. Using a modeling approach, including cell geometry and microtubule roles, we here offer a mechanism, which acts through microtubule dynamics.

We hypothesized that microtubule dynamics would be at the core of this novel regulation of cortical pulling forces, which would depend on spindle position. Delaying anaphase onset confirmed the existence of this positional control in *C. elegans*, and we subsequently directly observed astral microtubule availability at the cortex, especially in the posterior-most crescent. Combining the positional control of microtubule density with the posterior restriction of active force generators by the LET-99 band, we expanded the modeling of spindle rocking and positioning. We obtained and validated the dual control, *temporal* and *positional*, of pulling forces and took advantage of this so-called full-expanded model to dig into the robustness of the final spindle position, key for correct organism development. Interestingly, time simulations based on this model and our experiments suggest that spatial restriction of active force generators by the polarity factor LET-99 combined with microtubule dynamic instability limiting their contacts at the posterior-most cortex not only account for the final spindle position, but also suggest that details of microtubule number and motor number/dynamics contribute more modestly, ensuring a robust final spindle position.

MATERIALS AND METHODS

Culturing *C. elegans*

C. elegans nematodes were cultured as described in (26), and dissected to obtain embryos. All strains were maintained at 25°C, handled on nematode medium plates and fed with OP50 bacteria.

Strains

TH65 *C. elegans* (*Ce*) YFP::TBA-2 (α-tubulin) (27) and ANA020 *C. briggsae* (*Cb*) GFP::β-tubulin strains with a microtubule fluorescent labeling were used for the "landing" assay. TH27 *C. elegans* GFP::TBG-1 (γ-tubulin) (28) and *C. briggsae* ANA022 (GFP::TBG-1;GFP::HIS-11^{H2B}) strains (13), displaying a centrosomal fluorescent labeling, were the standards for the "centrosome-tracking" assay except for event timing. In that case, the

control was the *C. elegans* TH231 (SPD-2::GFP) strain with centrosome labeling crossed with OD56 (mCherry::HIS-58^{H2B}) histone labeling, which generated the JEP15 strain. This was then crossed with the KR4012 *such-1(h1960)* mutant strain (29) to create JEP16.

Gene silencing by RNA interference

RNAi experiments were performed by feeding, using bacterial clones from the Ahringer library (30) or ordered from Source BioScience. *let-99* exon3 was amplified from HT1593 genomic DNA and cloned into the L4440 plasmid. The feedings were performed at 25°C for various durations according to the experimental goals. When targeting proteins whose depletion led to changes in embryo size (*cid-1(RNAi), c27d9.1(RNAi), ani-2(RNAi)* and *ima-3(RNAi)*), we aimed for strong phenotypes and used a duration of 48h, except for *ima-3(RNAi)*, which was treated for 34h. For the other depletions by *RNAi* imaged at the spindle plane, we performed durations large enough to deplete the proteins and observe a phenotype, still having oscillations that could be quantified: the treatment lasted 6h for *spd-2* and *gpr-1/2*, and 24h for *par-3* and *let-99*. When investigating the residence time of the microtubules at the cortex, *gpr-1/2(RNAi)* and *par-3(RNAi)* were applied during 48h, *spd-2* 6h and *let-99* for 24h. We did not notice any phenotype suggesting that the meiosis was impaired during these various depletion experiments. When we aimed to change the embryo size by *RNAi*, we observed oscillation amplitudes similar to the untreated embryos, except after *ima-3(RNAi)*, for which we found that the oscillation amplitudes were very variable between embryos with amplitudes of the anterior centrosome similar to posterior centrosome's ones. The control embryos for the *RNAi* experiments were fed with bacteria carrying the empty plasmid L4440.

Quantitative Western Blotting

For measuring expression level of SPD-2, 50 adult gravid hermaphrodites were picked into 10 µl of M9 buffer and snap frozen in liquid nitrogen, then thawed, mixed with 10 µl sample buffer (180 mM Tris, [pH 6.8], 7,2% SDS wt/vol, 36% glycerol vol/vol, DTT 100mM), and loaded onto a Mini Protean TGX 4%–20% Tris-Glicine gel from BioRad. Immunoblots were probed using the primary anti-SPD-2 antibody MO750, kindly given by Prof. A.A. Hyman, at 1 mg/ml and detected using a horseradish peroxidase (HRP)-conjugated secondary antibody (1:5,000; Jackson ImmunoResearch) as described in (31). Quantification was performed using ImageJ after imaging the blot using an Amersham Imager 680 (GeHealthcare)

Preparation of the embryos for imaging

Embryos were dissected in M9 buffer and mounted on a pad (2% w/v agarose, 0.6% w/v NaCl, 4% w/v sucrose) between a slide and a coverslip. Depending on the assay, they were observed using different microscopic setups. To confirm the absence of phototoxicity and photodamage, we first checked for the normal rates of subsequent divisions before proceeding with further experimentation (32, 33).

Centrosome imaging

For the "centrosome-tracking" and the "event-timing" assays, embryos were observed at the spindle plane using a Zeiss Axio Imager upright microscope modified for long-term time-lapse. First, extra anti-heat and UV filters were added to the mercury lamp light path. Secondly, to decrease the bleaching and obtain optimal excitation, we used an enhanced

transmission 12 nm bandpass excitation filter centered on 485 nm (AHF analysentechnik). We used a 100x/1.45 NA Oil plan-Apo objective. Images were acquired with an Andor iXon3 EMCCD 512x512 camera at 33 frames per second and using Solis software. Embryos were imaged at 23°C. The beginning of the spindle's abrupt elongation (Fig. S4A in the Supporting Material) was used as the marker for anaphase onset (34), and the centrosome tracks of individual embryos were aligned using this time reference, for averaging purposes or for overlay on the "landing" assay. An exemplary event timing extraction is reproduced in Fig. S4C. Timings are summarized in Fig. S4D.

"Landing" assay

To measure the spatial distribution of microtubule cortical contact densities, fluorescent tubulin labeling of entire microtubules was used to observe both polymerizing and depolymerizing microtubules at the cortex of one-cell embryos at 23°C (Fig. 1D), using a spinning disk microscope (LEICA DMI6000 / Yokogawa CSU-X1 M1) equipped with an HCX Plan Apo 100x/1.4 NA oil objective. Illumination was performed by a white-light Fianium laser filtered around 514 nm using a homemade setup (35), sold by Leukos (Limoges, France). We subsequently de-noised the images by Kalman filtering (36), and detected microtubule contacts by applying u-track (37) (Fig. 1A-C). The recovered lifetimes of the microtubule contacts followed an exponential distribution as expected from a first order stochastic process (Fig. 1E) (19). To spatially map the microtubule contacts with a reasonable accuracy, for each embryo, we divided the cortex into ten regions of equal width along the anteroposterior (AP) axis and counted the number of contacts in each region along mitosis. The densities were computed by dividing these counts with the respective cortical region areas, which were precisely measured using the active contour algorithm (38). To gain certainty, we then performed averaging over 10-second blocks, since we observed minor changes of the microtubule contact density at that timescale. The final density map was obtained by averaging over embryos after the density maps were aligned temporally according to the onset of cytokinesis furrow ingression. This temporal cue was set when embryo shape decreases its convexity as reported by the ratio of convex area to active contour area (Fig. S4B). The landing assay is further detailed in the Supplementary Method in the Supporting Material.

Robustness plot

To assess the robustness of the position and timing of the posterior centrosomal oscillation onset against embryo length variations, we calculated dimensionless quantities (Fig. 4). For the timing, we used the reference duration *T* as being equal to the delay between two mitotic events independent of cell mechanics for control embryos. We chose the Nuclear Envelope BreakDown (NEBD) and the anaphase onset as these events. For each experiment, we computed t_0, the shift of the oscillation onset time with respect to the anaphase onset. The normalized shift $\overline{\delta t_0}$ was thus obtained by subtracting the corresponding mean value for control t_0^{ctrl} from the current value t_0, and by dividing the result by the reference duration: $\overline{\delta t_0} = \left(t_0 - t_0^{ctrl}\right) \big/ T$. We repeated this calculation for the positional quantities using the mean

embryo length L in control as a reference for normalization. For each experiment, we computed the shift of the position of oscillation onset, p_0, with respect to the corresponding control mean position p_o^{ctrl}. Normalization yielded the normalized shift of the oscillation onset position $\overline{\delta p_0} = \left(p_o - p_o^{ctrl}\right)/L$. We used a Student's *t*-test to see whether the linear fit slope was significantly different from 0. In doing so, we were able to determine whether e.g. embryo length had an impact on the position or timing being studied.

Simulation of the posterior displacement using the full-expanded model

We simulated the posterior displacement of the spindle using our full-expanded model with the TR-BDF2 algorithm (39). To ensure the proper force balance on the spindle poles, we also included the anterior centrosome in the full-expanded model and restricted the anterior active force generators' location to between 0 and 40% of the AP axis (15). We also kept the anterior centrosome at a fixed position for the sake of simplicity, making the spindle position dependent only on that of its posterior pole. On the anterior side, we used a two-fold lower force generator on-rate (14), resulting in half the number of active force generators compared to the posterior-most side (15). We assumed that force applied to posterior centrosome and originating in anterior side was halved after anaphase onset because sister-chromatids separated. We modeled the centering force with a spring (34) and used the processivity to control the progression of mitosis (16). Finally, since the model was linearized, it was limited to considering modest variations in parameters around their nominal values. This simulation is further detailed in the Supplementary Model in the Supporting Material.

Statistics

Averaged values were compared using a two-tailed Student's *t*-test with Welch Satterthwaite correction for unequal variance, except where otherwise stated. For the sake of simplicity, we recorded confidence levels using a diamond or asterisks (◊, p ≤ 0.05, *, $p \leq 0.01$; **, $p \leq 0.001$; ***, $p \leq 0.0001$; ****, $p \leq 0.00001$) and ns (non-significant, $p > 0.05$; sometimes omitted to save room). We abbreviated standard deviation to SD, standard error to s.e. and standard error of the mean to s.e.m.

Data processing, modeling, and simulation

All data analysis was developed using Matlab (The MathWorks). Modeling was performed using Wolfram Mathematica formal calculus software. Numerical simulations were performed using Matlab and Simulink (The MathWorks).

RESULTS

Astral microtubule contacts at the cortex depend upon centrosome position in *C. elegans*, enabling the spindle to sense its position.

To establish the nematode *C. elegans* as a suitable model, we first aimed to confirm that a positional control, *id est* a mechanism relating the cortical pulling force regulation to the spindle position, exists in this organism. Indeed, we previously reported that the position of

the spindle posterior pole controlled the onset of spindle oscillation in *C. briggsae* (13). In contrast with that nematode species, in which anaphase onset preceded oscillation by 30 s, in *C. elegans* these onsets were simultaneous. This could be coincidental, thus we tested whether a positional control exists in this latter by delaying anaphase. We used a *such-1*^{ANAPC5}*(h1960)* mutant of the anaphase-promoting complex/cyclosome (APC/C) (29), labeling centrosomes and chromosomes using SPD-2^{CEP192}::GFP; mCherry::HIS-58^{H2B}. We tracked the centrosomes (16, 34), and observed oscillations that started largely before anaphase in the mutant (Table 1) but occurred when the posterior centrosome was at 70.5% of embryo length, similarly to the control (70.0%). In contrast, for both strains, the die down of oscillations occurred just short of two minutes after anaphase onset, regardless of when oscillations started up, thus leading to different durations of the oscillation phase (Table 1). We conclude that a positional control of anaphase oscillation onset exists in *C. elegans* embryos, similarly to *C. briggsae*.

Previous studies have emphasized the key role of microtubules in the positioning of the microtubule-organizing center (MTOC). Indeed, they can "sense" cell geometry, for example to bring the MTOC to the cell center (40, 41), or to orient the nucleus by exerting pulling forces that scale with microtubule length (42). To challenge our hypothesis that the microtubule network provides a positional regulation of pulling forces, we decreased the microtubule nucleation rate through a mild *spd-2*^{CEP192}*(RNAi)* (27) (Movie S1-2 and Fig. S2E in the Supporting Material). The efficiency of this partial depletion was confirmed by Western blot (Fig. S2D), with the loss of SPD-2 equal to 59.4 ± 6.4% (N = 3 replicates) of the quantity measured in control conditions. By measuring the centrosome trajectories along cell division, we found that the posterior centrosome position at oscillation onset was significantly displaced posteriorly in SPD-2 depleted embryos, reaching 72.5% of embryo length compared to 70.1% in the control (Table 1). We checked that this change could not be attributed to a difference in the dynamics of the microtubules at the cortex and found no significant difference (Fig. S1C). We thus confirmed that astral microtubules, and likely their number contacting the cortex, play a role in regulating the centrosomal position at which oscillation begins.

Kozlowski and co-workers have reported that microtubules are not always abundant at any place at the cortex (19). We therefore hypothesized that the distribution of microtubule cortical contacts might depend on MTOC proximity, i.e. on centrosome position. We tested this by directly measuring microtubule distribution at the cortex ("landing" assay, Methods and Fig. 1D). We used α-tubulin labeling to view microtubules in both growing and shrinking states, the latter being present when microtubules are pulling from the cortex and not tracked by EB proteins. Since α-tubulin YFP::TBA-2 construct was added up to the endogenous copy and overexpressed due to the strong *pie-1* promoter (19), we checked that this labeling led to no phenotype with respect to the modeled traits. We compared the spindle pole trajectories as well as the oscillation amplitudes and timings of this entire-microtubule-labeled strain with those of the GFP::γ-tubulin centrosome-labeled strain (Fig. S1AB, Supp. Method). We did not observe any significant difference in these features, thus the model could be safely grounded on data measured in these two different strains. Because the microtubule dynamics are so fast,

we viewed the cortical contacts at a speed of 10 frames per second. This labeling combined with the fast acquisition led to images with a low signal-to-noise ratio, which required a powerful de-noising and adequate tracking (Supp. Method, Fig. 1A-C). We validated our image-processing analysis pipeline using simulated data (Fig. S1D-F, Supp. Method). We measured a histogram of microtubule contacting times at the cortex displaying an exponential distribution (Fig. 1E), characteristic of a first-order process, with a lifetime consistent with previously published values (19). We then calculated the spatial distribution of microtubule cortical contacts along the AP axis. To reduce uncertainty, we block–averaged the distribution in ten regions of equal width along the AP axis (Fig. 1D) and then performed a 10-second running average over the obtained density. The latter is possible because of the slower timescale associated with spindle displacement and microtubule dynamics regulation. The final density map was obtained by averaging the result over the embryos (Methods). Consistently, the associated standard errors of the mean were below 6% of the values themselves, except in the tip regions along the AP axis (#1 and #10, Fig. 1D) at early metaphase, where they could reach 20% because of a low count of microtubule contacts. We observed spatial heterogeneity with two high-density ridgelines and an overall increase in contacts between metaphase and anaphase, the latter being consistent with the increasing nucleation rate previously described (27) (Fig. 1F).

To test whether the high-density ridgelines could correspond to the centrosomal positions, we used a wide-field microscope to view the spindle plane in the same strain and at the same temperature, and tracked the centrosomes. We then combined the results from both experiments and aligned them temporally with anaphase onset (Methods and Suppl. Methods). We found that centrosome positioning coincides with the ridgelines (Fig. 2A). Since we had initially observed the positional switch on cortical pulling forces in one-cell *C. briggsae* embryos (13), we thus considered whether it could rely on a similar modulation of microtubule cortical contacts in space and time. We performed the same experiments in this species and obtained similar results (Fig. 1G and 2D). We conclude that the distance from the centrosome to the cortex strongly controls the number of microtubules contacting the cortex in both species.

In the posterior cortex, only the force generators localized in the posterior-most crescent (so-called the active region) are able to exert a pulling force on an astral microtubule. It is due to LET-99 inhibiting the force-generator pulling activity in the posterolateral region (distributed between 45% and 70% of the AP axis) (24), while preserving the twice larger number of active force generators on the posterior-most side of the embryo (11, 15). We propose that the displacement of the area where microtubule contacts are concentrated toward the posterior along the course of mitosis could increase the number of microtubule contacts in the active region — a means to regulate cortical forces. Could such a phenomenon create a positional switch? To address this question, we modeled the microtubule contacts at the cortex (Suppl. Model). While doing so, we included the dynamic instability of microtubules (43) and assumed for now that the force-dependence of the catastrophe rate was negligible (25). We also assumed that catastrophes happened only at the cortex (no free end catastrophe), and that microtubules fully depolymerized upon shrinking (negligible rescue rate) (19, 27, 44). We set

a constant number of microtubule nucleation sites at the centrosomes, neglecting the modest increase in nucleation rate observed during anaphase compared to metaphase (27). Furthermore, these nucleation sites were never empty (25), and the microtubules emanated from there in an isotropic angular distribution (27, 45). We computed the number of microtubules that reached the cortex in the active region as a function of the position of the posterior centrosome (Fig. 2B, black curve). This highlighted a limited number of microtubule cortical contacts when the centrosome position was close to cell center, with an initial slow increase in this number upon posterior displacement, followed by a steeper increase so that a high level was reached at close to 70% of embryo length, consistent with the onset of oscillation observed at that position. To confirm, we sought to measure microtubule contacts in the active region experimentally, counting them in our "landing" assay and obtaining a consistent measurement (Fig. 2C). We propose that microtubule dynamics are at the core of the experimentally observed positional switch by regulating the number of microtubules available to force generators, making it dependent on centrosome position. Furthermore, the large number of microtubules that reach the active region during mid and late anaphase is consistent with the initial model's assumption that microtubules saturate a limited number of cortical force generators during this phase (16, 17). The restriction of active force generators to a posterior crescent smaller than the embryo half, probably by LET-99, is key to this modeling result. Overall, it paves the way towards understanding the positional regulation of the cortical pulling forces involved in spindle rocking, posterior displacement and elongation.

Microtubule cortical contact modulation exerts a positional control on the number of engaged force generators

To quantitatively investigate how varying microtubule cortical contact density interacts with spindle position to regulate cortical pulling forces, and to further study the subsequent impact on final spindle position, we further developed the physical modeling and extended our initial model (16). We propose that two modules combine to regulate the pulling forces (Fig. 3A). In the first module, the position of the posterior centrosome is linked to the number of microtubule cortical contacts in the active region, which is, in turn, able to limit the number of engaged force generators, as modeled in the previous section. The second module provides a temporal/mitotic progression control of the pulling forces through the dynamics of the force generators (16, 18, 46). Up to now, only the latter was accounted for in the initial model, and we envisioned that combining with the former would unravel novel robustness in the regulation of pulling forces, and in doing so would reveal the mechanism linking cortical polarity and final spindle position.

We created a first version of this two-module model, termed "expanded model," where we continued to neglect the temporal evolution of force generator processivity (Fig. 3A). We modeled the binding of microtubule and dynein as a first-order chemical reaction using the law of mass action, assuming no cooperative binding between force generators (47), and estimated the association constant from the binding and unbinding rates used in the initial model (16) (Suppl. Model). This enabled us to compute the number of engaged force generators versus the posterior centrosome position (Fig. 3B, black line). We found that when the centrosome was far from the posterior tip, we observed a scarcity of astral microtubules contacting the cortex in its active region, which limited the number of engaged force

generators to below the previously described threshold for oscillating (16). Upon posterior displacement of the centrosome, beyond 60% of the AP axis, we observed a steep increase in engaged force generator count, similar to the one found in the number of microtubule cortical contacts (compare the black curves in Fig. 2B and 3B). This was followed by a saturation starting from 70% of the AP axis because of the limited number of active force generators. These two successive regime changes created a switch, which was consistent with our positional control hypothesis. In conclusion, our expanded model predicts that oscillation onset — a readout of pulling force increase — is regulated by posterior displacement of the posterior centrosome.

We experimentally challenged the expanded model in three ways related to each biological player (Fig. 3A, top line) through measuring the timing of oscillation onset with respect to anaphase onset, and the posterior centrosomal position when oscillation starts. Firstly, we varied the extent of the active force generator region in the expanded model and could predict that the precise position at which oscillations start correlates with the boundary of the active region (Fig. 3B). The extent of this region inversely reflects the LET-99 cortical band (24). We thus increased this extent towards the anterior side, still in the embryo's posterior half, by partially depleting LET-99. We observed that as compared to the control, the position of the posterior centrosome at which oscillations began was significantly displaced towards the anterior (Fig. 3C), in agreement with the expanded model's predictions (Fig. 3B, blue and green curves). We checked for no change in microtubule residence time at the cortex (Fig. S1C), consistently with the model priors. To gain certainty, we impaired the cortical domain boundary in a different manner: upon *par-3(RNAi)*, we expected PAR-1 domain to extend more towards the anterior pole so that the LET-99 band would be more anterior (48). We observed that in such a condition, the posterior centrosome started oscillation much more anteriorly than in control embryos (Fig. 3D). This change could not be the consequence of the increased microtubule lifetime at the cortex upon *par-3(RNAi)* (Fig. S1C) as it would result in an opposite effect (Fig. M4E in the Suppl. Model). Based on these two experiments in which the active region extended more anteriorly than in the untreated embryos, we conclude that the position of the active region boundary controls the position where oscillation onset occurs.

In a second prediction challenging experiment, we focused on microtubules and predicted that a decrease in their total number emanating from either centrosome would posteriorly displace the position of oscillation onset (Fig. S2A, blue and green curves). Experimental depletion of the protein SPD-2 by *RNAi* decreased microtubule nucleation at the centrosomes (27) and resulted, as predicted, in a posteriorly shifted position of the posterior centrosome at oscillation onset (Table 1).

Thirdly, we varied the number of active force generators, which is predicted to have a reduced impact on the oscillation onset (Fig. S2B, green curve), provided that it was above the needed threshold (16). We previously observed that the oscillation onset position was not significantly changed in *gpr-1(ok2126)* or *gpr-2(ok1179)* mutants (13). We set to reproduce this result in the present paper using a partial *gpr-1/2(RNAi)*. To estimate the remaining level of force generation, we observed the posterior centrosome oscillations and noted a reduction of their amplitude to 11.4 ± 6.3% of embryo width (mean ± S.D., N = 19 embryos, p = 9.7×10^{-3}) compared to 16.1 ± 3.5% (N = 10), as expected (11). Under that condition, the

position at which the oscillations began was not significantly altered (Fig. S2C). Importantly, the residence time of the microtubules at the cortex was not affected in this condition (Fig. S1C). Overall, these three results support our model: microtubule dynamics sense centrosome position and the extent of the active region, which in turn controls the position triggering oscillation onset.

The position at which pulling forces burst is resistant to variations in embryo length.

Since the astral microtubules can sense the distance from the centrosomes to the cortex, the proposed mechanism may also make the positional regulation of the cortical pulling forces dependent on the cell geometry. To this respect, it could be reminiscent of the yeast positional check point (49), as well as the adaptation of cell division plane positioning to variations in cell shape observed in other contexts and organisms (42, 50, 51). Our expanded model suggested that the posterior centrosome position at oscillation onset is only weakly dependent upon the length of the embryo (Fig. 4A). To experimentally investigate this prediction, we depleted C27D9.1 by *RNAi* to obtain longer embryos, and performed *cid-1(RNAi)*, *ima-3(RNAi)* or *ani-2(RNAi)* to yield shorter ones (Fig. 4B). In all cases, the imaged embryos were viable. Embryos with depleted IMA-3 displayed an altered oscillation phenotype, with a large variability in the centrosome oscillation amplitudes between embryos and with anterior and posterior centrosomes displaying similar amplitudes. We measured normalized variations in the timing and positioning of oscillation onset with respect to the variations in embryo length and computed the shifts from control averages (Methods). For both temporal and positional analyses, we fitted a linear regression, measuring oscillation onset timing slope 5.6 times larger than that of the oscillation onset position (Fig. 4CD). It was indicative that the positional switch at about 70% of the AP axis was conserved despite variations in embryo length. Consistently, the position shift spread around the fitted line was narrower in comparison to normalized oscillation onset time shift. This was expected as the position of oscillation onset is regulated thus constrained, as suggested by the proposed model, and depends on quantities mostly independent of embryo length, whereas its timing is unconstrained and could thus vary in a broader range. The very low slope of the linear regression in Fig. 4C suggested that the positional control could make the position at which cortical force bursts resistant to changes in embryo length. Interestingly, Farhadifar *et al.* showed that both the final spindle length and the division plane position scale linearly with embryo length within different *C. elegans* natural isolates, and beyond within several nematode species (52). These correlations may be either enforced by natural selection or due to some robustness mechanisms, two non-exclusive possibilities. Since the cortical pulling forces play an important role in setting the spindle length and positioning the division plane, the positional regulation exhibited here may be one of the mechanisms accounting for such a robustness. In contrast, we showed that the timing of oscillation onset displayed a positive correlation with embryo length, with a larger linear regression slope than the one measured for the position. This is consistent with longer embryos requiring a larger duration of posterior displacement to reach the critical 70% of the AP axis position for oscillation onset (13). Overall, it also supports the idea that the positioning and timing of oscillation initiation are not connected at anaphase onset.

Centrosome position and time/mitotic progression both contribute to oscillation and pulling force regulation.

We found that the oscillation onset is controlled by the position of the posterior centrosome while its die down timing is dependent on the time control (mitotic progression). Beyond these dominant effects, however, we also noticed that oscillations might start while the centrosome was close to 70% of the AP axis, rather than when it reached this position (Table 1). We suspected that a combination of both temporal and positional controls was at work. We set to recapitulate this regulation by completing our model and validating it. We included the temporal control within the expanded model, as previously done in the initial model, i.e. through the decrease of microtubule force-generator detachment rate (off-rate), which is the inverse of processivity (16). Doing so, we made the microtubule–force generator equilibrium-constant dependent on time through the decreasing off-rate. We will from now refer to this model as the "full-expanded model" (Suppl. Model). In contrast to the initial model, the force generator on-rate is no longer constant and instead depends on the number of microtubules available at the cortex for binding a force generator, and on the extent of the active region. It also depends on the on-rate imbalance reflecting polarity (14). Using the full-expanded model, we computed the stability diagram corresponding to centrosome oscillation, which depended on both temporal and positional control parameters: the force generator processivity and the position of the posterior centrosome, respectively. Non-stable region (Fig. 5A, blue region) corresponded to model parameter sets in which oscillation developed. In contrast, in stable regions (Fig. 5A, white regions), the system was overdamped, causing pre-existing oscillations to die down. This diagram suggested that to enable oscillation, in addition to a large enough force generator processivity (16), the posterior centrosome needed to be close enough to the posterior tip of the embryo, which supported our positional switch hypothesis investigated above (Fig. 5A, thick blue curve), leading to a dual control of the pulling force outburst. While this model offered a clear view about oscillation onset, we could only infer predictions of oscillation die down from the return-to-stability curve, which corresponded to when the system starts dampening out oscillation (Fig. 5A, green curve). This was because no detailed model relates mitotic progression/time to processivity. Interestingly, the steeper slope of this return-to-stability curve compared to the oscillation onset curve suggested that the posterior centrosome position was likely to more strongly influence oscillation onset than die down (Fig. 5A). This was consistent with the equal anaphase-onset to oscillation-die-down duration observed in *such-1(h1960)* mutant and its control (Table 1).

To challenge this full-expanded model, we again experimentally investigated the role of players in each regulation (Fig. 3A). We first observed that an anterior shift of the boundary position of the active region by *let-99(RNAi)* or *par-3(RNAi)* did not alter the oscillation die down timing significantly with respect to the control, while oscillation onset happened not only earlier (Fig. 5BC), but more importantly, when the posterior centrosome was positioned more anteriorly (Fig. 3CD). This was consistent with model predictions (Fig. 5A, dashed blue line) and expected since oscillation die down depended on time control (Fig. 3A). Secondly and in contrast, we decreased the number of active force generators at the cortex by *gpr-1/2(RNAi)*, and measured a precocious oscillation die down (Fig. 5D), while oscillation onset position was unchanged (Fig. S2C). This result was predicted by the model, disregarding

whether we modeled the decrease in active force generators through their number (11, 15) or their on-rate binding to microtubules (14) (Fig. 5A, chain and continuous thin blue lines, respectively). Overall, the full-expanded model correctly accounted for phenotypes resulting from perturbations affecting a player either related to the positional module or the time module (Fig. 3A). Interestingly, the resulting phenotype was affecting mostly either the posterior centrosome position at oscillation onset or the timing of oscillation die down, but not both, suggesting some independence of the two pathways, likely caused by the different players involved in each regulation. This dual regulation calls for a re-examining of how the final position of the spindle is set, superseding the initial model, in which we proposed that only the force generator number and dynamics contributed (16).

LET-99 spatial restriction of active force generators sets the final spindle position.

Equipped with the full-expanded model grounded on the analysis of oscillation onset, we used it to investigate the mechanism connecting the cortical polarity, through its downstream effector LET-99, to the final centrosome positions. Indeed, the final positions of both the spindle poles and center set the position of the cytokinesis furrow (8). Their positions depend upon cortical pulling forces and therefore the positional and temporal controls over these forces were expected to contribute to the robustness of the final spindle position. In contrast, in our initial model, we suggested that the final posterior centrosome position resulted from a balance between the cortical pulling forces and centering forces, the latter being modeled by a spring (16, 34). In a broader take, this is the current paradigm disregarding the detail of the centering mechanism (9, 53). To investigate final spindle positioning, we simulated the posterior displacement using our full-expanded model (Methods). We could reproduce the global kinematics of posterior displacement: slow prior to anaphase then accelerating afterward (Fig. S3E) as we previously observed experimentally (34).

The polarity factor LET-99 sets the boundary of the active region and was proposed to set the final spindle position downstream of polarity (23, 24). We foresaw that the full-expanded model proposed here could recapitulate the mechanism of this control. To test this, we simulated posterior centrosome displacements during mitosis with different boundary positions of the active region and observed that the final position of the posterior centrosome was displaced anteriorly when the boundary of the posterior active crescent moved anteriorly, so long as the region was large enough to initiate posterior displacement in the first place (Fig. 6D, solid lines). This result was confirmed experimentally in *let-99(RNAi)*- or *par-3(RNAi)*-treated embryos (Fig. 6AB), and is consistent with previous observations (24). This prediction and our experimental observations differed from the initial model ones, which stated that under similar cortical forces, the posterior displacement would be the same disregarding the cortical distribution of the force generators (Fig. 6D, dashed line).

LET-99 may act either by concentrating force generators in the posterior active region or by spatially restricting them to a posterior-most crescent. To decide between these mechanisms, we tested how sensitive the centrosome final position was with respect to the precise final count or dynamics of the force generators. In particular, we investigated the impact of the total number of force generators available (Fig. 6F), of their final detachment rate (off-rate) that reflected the time/mitotic progression control (Fig. 6G), and of their binding rate to

microtubules (on-rate), which was recently suggested to reflect polarity (14) (Fig. 6E). In this latter case, we scaled up or down the on-rate in similar ways on both the anterior and posterior. Our time simulations of posterior centrosome displacement suggested a reduced dependency on force generator characteristics, in contrast with the initial model, provided that a threshold force was reached to enable posterior displacement. Experimentally, we observed that a hypomorphic *gpr1/-2(RNAi)* induced a partial reduction of the cortical forces (11, 15) and caused no significant shift in final spindle position (Fig. 6C). This robustness of the full-expanded model was attributed to a smaller increase in cortical pulling forces after crossing the boundary position of the active region (Fig. S3D), since the increasing processivity was tempered by a saturation of microtubule contact count in mid-anaphase. Along the same line, the force generator final processivity was likely disturbed in *such-1(h1960)*, the mutant with delayed anaphase onset (18), and as predicted, the final position of the posterior centrosome was conserved (Table 1).

Microtubules are key players in our positional mechanism and are proposed to contribute to anaphase oscillation through a modulation of their cortical contact counts (19). We thus wondered how important the total number of microtubules was in setting the final spindle position. We simulated posterior centrosome displacements with a scaling down of microtubule number and observed that, above a microtubule-count threshold needed for posterior displacement, their precise number was again unimportant (Fig. 6H). Consistently, we found no strong alteration of posterior centrosome final position upon partially depleting SPD-2 when compared to the shift measured in its position at oscillation onset (Table 1). Interestingly, we also observed an optimum value in microtubule count to maximize the posterior displacement (Fig. 6H, red and green curves below the black one). We overall conclude that the proposed mechanism, in which the distribution of force generators is spatially restricted to the posterior-most crescent, perfectly accounts for the connection between the LET-99 band and the final position of the posterior centrosome, and consequently of the spindle (Fig. 3A, yellow). Furthermore, it also suggests that this position is resistant to modest changes in the parameters related to microtubules or force generators, as long as they reach threshold values needed for posterior displacement of the spindle.

DISCUSSION

We measured the spatial distribution of microtubule contacts at the cell cortex and found it uneven, with higher concentrations of microtubule contacts in the regions closest to the centrosomes. As a direct consequence and in combination with the restriction of cortical pulling force generation to a posterior-most crescent (24), the number of microtubules available to cortical force generators displayed a strong increase linked to the posterior spindle displacement, with a switch-like behavior. This in turn made the cortical pulling forces dependent on the position of the centrosomes. Thus, astral microtubule dynamics create a *positional* control over pulling forces, especially over their burst at anaphase onset, revealed by spindle oscillations. We quantitatively recapitulated this novel regulation into an expanding of our initial model of spindle oscillation and posterior displacement (16). This positional regulation superimposes firstly to the force imbalance, reflecting polarity, and essential for the spindle to be displaced posteriorly (11, 15, 54), and secondly to the *temporal* control related to mitotic progression (18), which sets the velocity of displacement and

consequently its duration. To this respect, in *C. briggsae*, we observed lower amplitude oscillation and a 30-second delay in posterior centrosome reaching 70% of embryo length (13).

The various aspects of the regulation of pulling forces during the first division of *C. elegans* embryo, namely temporal, positional and polarity related, have been investigated independently using modeling while here, in contrast, we have recapitulated these regulations in a sole model. Although built on these previous results, our proposed model displays differences and we discuss these with respect to four important aspects. (i) Our model is an expansion of our previous temporal regulation focused model (16). In both cases the positive feedback needed to permit oscillations was due to the load-dependent detachment rate and force-velocity relation undergone by the force generators. It results in a larger persistence of force generator pulling on the microtubule, as the centrosome gets closer to the "winning side" of the cortex. In contrast, Kozlowski *et al.* suggested a positive feedback mostly due to the inability of the microtubules to reach the "losing side" of the cortex (19). Both mechanisms may supplement each other although we did not observe a variation of the microtubule contacts on the time scale of oscillations and therefore favored the positive feedback due to force generator dynamics. (ii) In our model, the limited accessibility of microtubules to the cortex rather contributes to the positional regulation. Importantly, although we share a similar law for microtubule accessibility to the cortex with the Kozlowski's model, we supplemented this regulation with the temporal one – a novel feature. We showed in particular that both temporal and positional aspects play an independent role in regulation. This is also a distinctive feature from the model proposed by Kimura and Onami, where the release of the repression of half of the posterior force generators needed to ensure the imbalance of the number of active force generators, is suggested to be under mitotic progression, i.e. time control (55). In our case, the limit of the number of engaged force generators is released by the posterior displacement of the spindle making more microtubules contact the cortex, thus exerting a positional control. Doing so, our model well accounts for the delayed oscillation when the embryos are larger as seen e.g. in *C. briggsae*. A temporal regulation would rather produce oscillations at the same time as in normal-length embryos and therefore more anteriorly. (iii) In contrast with the proposed model where the final position of the spindle mainly reflects the extent of the region devoid from LET-99, it was previously proposed to result from the balance of centering forces modeled in various fashions and cortical pulling. This latter case requires precise tuning of these forces to ensure a correct and reproducible final position of the spindle (9). This means that the mechanism centering the spindle, and the related cell geometry, contributes substantially to determining the final spindle position. In particular, a dependence of pulling forces on the spindle eccentricity was previously proposed (56) combining similar aspects to ours, namely the 3D modeling of astral microtubules, isotopically emanating from the centrosome and contacting the cortex where a limited number of active force generators are present. However, since Grill and coworkers assumed that microtubules are always abundant at the cortex, contrasting with our density measurements during metaphase, it creates a force contributing to center the spindle (53, 56). Interestingly, such a phenomenon is present in our model and likely contributes to limit the posterior displacement when the spindle is posterior enough, thus

microtubules abundant at the cortex. It may account for the robust final positioning in spite of modest variations of the number of microtubules or force generators. But beyond that, we here propose an original robust mechanism ensuring a faithful positioning with respect to cortical polarity cues through LET-99 (24), requiring a minimal number of active forces generators but no tight regulation beyond that threshold. As a result, it accounts for a reduced dependency on the centering force (Fig. M5B in the Suppl. Model). (iv) Finally, in our modeling, we have assumed an end-on attachment of the microtubules at the cortex as it corresponded to our and previous observations (19, 57). Indeed, side-on attachment was proposed to contribute to pronuclei centering prior to mitosis (58) and was also observed during telophase. However, the spindle displacement ends earlier than this switch in microtubule attachment. In conclusion, our model stands on and expands previous ones, altering the priors when experiments suggest to.

The identified dual regulation of the cortical pulling forces perfectly accounts for the robustness of the final spindle positioning. We prove that restricting spatially force generation to a posterior-most crescent is key, while the precise level of active force generators or microtubule contacts at the cortex is of lower importance. By precise level, we mean that minimal numbers of microtubules and active force generators are required to ensure posterior displacement, but beyond that constraint, the values do not need to be finely tuned and modest variations can be buffered. Understanding robustness by accounting for a spatial distribution and regulation of force generation is, in its principle, similar to the contribution of both the asymmetric microtubule array and a LET-99 band to force regulation during centration and orientation of the pronuclei-centrosome complex (59). Indeed, we propose here that the mechanism linking the LET-99 domain and final spindle position relies on spatial restriction of active force generators to a posterior-most crescent. In contrast, and because the final spindle position is robust to modest variations of active force generator count, it is unlikely that LET-99 acts by concentrating the force generators in the posterior-most crescent. The imbalance in force generator number, reflecting GPR-1/2 posterior concentration (12, 13), is likely unrelated to the LET-99 band. Consistently, an extra shift of final spindle positioning towards the anterior pole was observed previously upon treating a *let-99(or81)* mutant with *gpr-1/2(RNAi)* (60).

The positional control of cortical pulling forces also contributes to ensuring the correct positioning of the cytokinesis cleavage furrow, essential for the correct distribution of cell fate determinants (1, 2, 5). Indeed, in late mitosis, furrow position is signaled by two parallel pathways: firstly, by the spindle poles through astral microtubules and secondly by the central spindle (61). For the latter, the signaling comes from the central spindle position when the spindle has reached its full elongation, which is controlled by the microtubule pulling forces (62). Overall, by regulating the position of the posterior centrosome and where pulling force burst causing elongation occurs, the proposed mechanism, based on microtubule network sensing cell geometry, contributes to robustness to the cleavage furrow positioning.

Quantitative genetic studies in *C. elegans* have found an approximately threefold lower persistence of new mutations on the phenotypic trait positioning the division plane compared to the trait displaying the time between first oscillation peak and mid-elongation (52). We

here measured the related parameter, duration of oscillations. As explained above, peak amplitude corresponds to the return–to–stability in our diagram (Fig. 5A) and behaves similarly to oscillation die down. We found final spindle position with a reduced dependency on variations in force generator number and dynamics compared to oscillation timings, as reported by e.g. oscillation duration. This is consistent with the proposed robustness mechanism de-correlating the final spindle position, likely essential to viability, from timings that appear less evolutionary constrained. Along the same line, we recently performed a comparative study between two nematode cousins (*C. elegans* and *C. briggsae*) (13). Because of a duplication of the regulators of force generators in *C. elegans*, GPR-1 and GPR-2, while *C. briggsae* only displays GPR-2, the pulling force regulation is altered leading to a delay in posterior displacement in the latter species. Here, the posterior centrosome arriving at 70% of the AP axis is delayed by 30 s and so is the oscillation onset, both with respect to anaphase onset. In contrast, the oscillation die down timing is correlated with that of anaphase onset in both species. Our dual control, position and time, perfectly accounts for the buffering of timing differences in centrosome kinematics, to ensure robust oscillation onset positions and similar final spindle positioning in both species. The evolution of the essential *gpr* genes between *C. elegans* and *C. briggsae* was likely made possible by the positional control and the resulting resistance to variations in force generator quantity and dynamics. Interestingly, cross-species insertion of *gpr* genes modulates oscillation amplitude but preserves the positional control, which is consistent with our *gpr-1/2(RNAi)* experiment (13). The robustness of final spindle positioning is therefore likely to be true in more than just these two species.

Finally, the observed positional switch is caused by astral microtubules, and more precisely by the number of microtubule cortical contacts, which reflects the distance between the centrosome and the cortex. Indeed, said distance is measured in “units of microtubule dynamics.” Astral microtubules provide feedback about the posterior centrosome position to the cortical pulling forces which suggests the existence of a mechano-sensing pathway. Such a property already enables classic mechanisms for creating centering (41, 63) or other shape-dependent regulation (42, 64, 65). However, such mechanisms were mostly inferred from cell-level measurements. In contrast, here, the distribution of the microtubule-end contacts located at the cortex was obtained from microscopic measurements. We observed a density ratio of approximately two between the regions with the most and least microtubule contacts at a given time, and this ratio represents the sensitivity to centrosomal position. From a theoretical point of view, considering the ellipsoidal shape of the *C. elegans* embryo and the microtubule dynamics measurements performed elsewhere, the predicted maximal ratio is 1.64 (Suppl. Model). Our experimental result is close to this prediction, suggesting that the microtubule dynamics parameters are optimal for the positional control that we discussed here.

CONCLUSION

This study of pulling force regulation by the mitotic spindle position was grounded in modeling and experimentally studying the microtubules at microscopic– and cell–scales. This was supplemented by investigating the precise timing of transverse oscillation onset with respect to anaphase onset and posterior centrosome positioning at that moment in the *C.*

elegans embryo. It has highlighted the key role of microtubule dynamics in probing the boundary of the active force generator region. In particular, microtubules create a *positional* control on spindle oscillations, which acts in addition to the previously described regulation by pulling force generator dynamics (*temporal* control). Both controls contribute independently to the switch to prevent premature pulling force burst. The finding of this supplementary positional control paves the way to a novel understanding of the mitosis choreography mechanism, supplementing the regulation by the cell cycle.

In particular, our proposed positional control connects the final spindle position to cortical polarity cues. Indeed, LET-99 spatially restricts the force generators to a posterior-most crescent, and in turn, microtubule dynamics read out the boundary of this region to properly position the centrosomes and thus the spindle at the end of mitosis. Interestingly, it also makes this position resistant to modest variations in microtubule quantity or in force generator dynamics or number, provided that these are above the required thresholds, guaranteeing correct cytokinesis furrow positioning and consequently a proper distribution of cell fate determinants (3, 4). Such a robustness buffered changes in cortical pulling force levels and timings between the *C. elegans* and *C. briggsae* nematodes, and permitted substantial modifications in the essential *gpr-1/2*^{LGN} genes, whose proteins are part of the complex that generates cortical pulling forces (13). Finally, the observed positional switch is caused by astral microtubules. They provide feedback about the posterior centrosome position with respect to the posterior-most crescent boundary, through the cortical pulling forces, suggesting the existence of a mechano-sensing pathway. This finding is a novel example of a microfilament-based system that controls essential aspects of cell division. In contrast with robustness resulting from classic biochemical signaling pathways (66, 67), this mechanism is based solely on cell mechanics and component dynamics.

ACKNOWLEDGMENTS

The SPD-2 antibody was a kind gift from Prof. Anthony A. Hyman. We thank Dr Grégoire Michaux for the feeding clone library and technical support. We also thank Drs Benjamin Mercat, Anne Pacquelet, Xavier Pinson, Yann Le Cunff, Grégoire Michaux, Roland Le Borgne, Sébastien Huet, Marc Tramier, Claude Prigent, Sylvie Tournier, Françoise Argoul, and Alain Arnéodo for technical help, critical comments on the manuscript, and discussions about the project. JP was supported by a CNRS ATIP starting grant and *La ligue nationale contre le cancer*. We also acknowledge *plan cancer* grant BIO2013-02, COST EU action BM1408 (GENiE) and *la ligue contre le cancer (comités d'Ille-et-Vilaine et du Maine-et-Loire)*. Some strains were provided by the CGC, which is funded by NIH Office of Research Infrastructure Programs (P40 OD010440; University of Minnesota, USA). Microscopy imaging was performed at the MRIC facility, UMS 3480 CNRS / US 18 INSERM / University of Rennes 1. Spinning disk microscope was co-funded by the CNRS, *Rennes Métropole* and *Region Bretagne* (AniDyn-MT grant). HB's postdoctoral fellowship was funded by *Region Bretagne* (AniDyn-MT grant) and the European Molecular Biology Organization.

AUTHOR CONTRIBUTIONS

Conceptualization, JP, HB, and MD; Methodology, HB, LC, and JP; Software, JP and HB; Validation / Formal Analysis, HB, SP, and LC; Investigations / Data Curation, HB, SP, LC,

DF, and JP; Writing – Original Draft, HB and JP; Writing - Review & Editing, HB, LC, MD, DF and JP; Supervision, JP.

SUPPORTING MATERIAL

An online supplement to this article can be found by visiting BJ Online at http://www.biophysj.org, with the material listed below:

- Figure S1: Validation of the strain and the analysis pipeline used to measure microtubule contact density at the cell cortex.
- Figure S2: Microtubule number affects the oscillation onset position, while force generator quantity above a threshold does not.
- Figure S3: Simulation of the displacement of the posterior centrosome using the full-expanded model.
- Figure S4: Landmarks used to set reference times and oscillation characteristics.
- Table S5: Parameters used for modeling and simulations.
- Supplemental Methods: The “landing” assay.
- Movie S1: Spindle positioning in a *C. elegans* control embryo.
- Movie S2: Spindle positioning in a reduced-microtubule-nucleation embryo.
- Supplemental Model.

SUPPORTING REFERENCES

References (68-84) appear in the Supporting Material.

REFERENCES

1. Betschinger, J., and J. A. Knoblich. 2004. Dare to be different: asymmetric cell division in Drosophila, *C. elegans* and vertebrates. Curr Biol 14:R674-685.
2. Gillies, T. E., and C. Cabernard. 2011. Cell division orientation in animals. Curr Biol 21:R599-609.
3. Gonczy, P. 2008. Mechanisms of asymmetric cell division: flies and worms pave the way. Nat Rev Mol Cell Biol 9:355-366.
4. Morin, X., and Y. Bellaiche. 2011. Mitotic spindle orientation in asymmetric and symmetric cell divisions during animal development. Dev Cell 21:102-119.
5. White, E. A., and M. Glotzer. 2012. Centralspindlin: At the heart of cytokinesis. Cytoskeleton (Hoboken) 69:882-892.
6. Rappaport, R. 1971. Cytokinesis in animal cells. Int Rev Cytol 31:169-213.
7. Knoblich, J. A. 2010. Asymmetric cell division: recent developments and their implications for tumour biology. Nat Rev Mol Cell Biol 11:849-860.
8. Bringmann, H., and A. A. Hyman. 2005. A cytokinesis furrow is positioned by two consecutive signals. Nature 436:731-734.
9. McNally, F. J. 2013. Mechanisms of spindle positioning. Journal of Cell Biology 200:131-140.
10. Nguyen-Ngoc, T., K. Afshar, and P. Gonczy. 2007. Coupling of cortical dynein and G alpha proteins mediates spindle positioning in *Caenorhabditis elegans*. Nat Cell Biol 9:1294-1302.
11. Colombo, K., S. W. Grill, R. J. Kimple, F. S. Willard, D. P. Siderovski, and P. Gonczy. 2003. Translation of polarity cues into asymmetric spindle positioning in *Caenorhabditis elegans* embryos. Science 300:1957-1961.

12. Park, D. H., and L. S. Rose. 2008. Dynamic localization of LIN-5 and GPR-1/2 to cortical force generation domains during spindle positioning. Dev Biol 315:42-54.
13. Riche, S., M. Zouak, F. Argoul, A. Arneodo, J. Pecreaux, and M. Delattre. 2013. Evolutionary comparisons reveal a positional switch for spindle pole oscillations in *Caenorhabditis embryos*. J Cell Biol 201:653-662.
14. Rodriguez Garcia, R., L. Chesneau, S. Pastezeur, J. Roul, M. Tramier, and J. Pecreaux. 2017. Dynein dynamics at the microtubule plus-ends and cortex during division in the *C. elegans* zygote. bioRxiv:118604.
15. Grill, S. W., J. Howard, E. Schaffer, E. H. Stelzer, and A. A. Hyman. 2003. The distribution of active force generators controls mitotic spindle position. Science 301:518-521.
16. Pecreaux, J., J. C. Roper, K. Kruse, F. Julicher, A. A. Hyman, S. W. Grill, and J. Howard. 2006. Spindle oscillations during asymmetric cell division require a threshold number of active cortical force generators. Curr Biol 16:2111-2122.
17. Grill, S. W., K. Kruse, and F. Julicher. 2005. Theory of mitotic spindle oscillations. Phys Rev Lett 94:108104.
18. McCarthy Campbell, E. K., A. D. Werts, and B. Goldstein. 2009. A cell cycle timer for asymmetric spindle positioning. PLoS Biol 7:e1000088.
19. Kozlowski, C., M. Srayko, and F. Nedelec. 2007. Cortical microtubule contacts position the spindle in *C. elegans* embryos. Cell 129:499-510.
20. Espiritu, E. B., L. E. Krueger, A. Ye, and L. S. Rose. 2012. CLASPs function redundantly to regulate astral microtubules in the *C. elegans* embryo. Dev Biol 368:242-254.
21. Gonczy, P., J. M. Bellanger, M. Kirkham, A. Pozniakowski, K. Baumer, J. B. Phillips, and A. A. Hyman. 2001. zyg-8, a gene required for spindle positioning in *C. elegans*, encodes a doublecortin-related kinase that promotes microtubule assembly. Dev Cell 1:363-375.
22. Tsou, M. F., A. Hayashi, L. R. DeBella, G. McGrath, and L. S. Rose. 2002. LET-99 determines spindle position and is asymmetrically enriched in response to PAR polarity cues in *C. elegans* embryos. Development 129:4469-4481.
23. Wu, J. C., E. B. Espiritu, and L. S. Rose. 2016. The 14-3-3 protein PAR-5 regulates the asymmetric localization of the LET-99 spindle positioning protein. Dev Biol 412:288-297.
24. Krueger, L. E., J. C. Wu, M. F. Tsou, and L. S. Rose. 2010. LET-99 inhibits lateral posterior pulling forces during asymmetric spindle elongation in *C. elegans* embryos. J Cell Biol 189:481-495.
25. Howard, J. 2006. Elastic and damping forces generated by confined arrays of dynamic microtubules. Phys Biol 3:54-66.
26. Brenner, S. 1974. The genetics of *Caenorhabditis elegans*. Genetics 77:71-94.
27. Srayko, M., A. Kaya, J. Stamford, and A. A. Hyman. 2005. Identification and characterization of factors required for microtubule growth and nucleation in the early *C. elegans* embryo. Dev Cell 9:223-236.
28. Oegema, K., A. Desai, S. Rybina, M. Kirkham, and A. A. Hyman. 2001. Functional analysis of kinetochore assembly in *Caenorhabditis elegans*. The Journal of Cell Biology 153:1209-1226.
29. Tarailo, M., R. Kitagawa, and A. M. Rose. 2007. Suppressors of spindle checkpoint defect (such) mutants identify new mdf-1/MAD1 interactors in *Caenorhabditis elegans*. Genetics 175:1665-1679.
30. Kamath, R. S., A. G. Fraser, Y. Dong, G. Poulin, R. Durbin, M. Gotta, A. Kanapin, N. Le Bot, S. Moreno, M. Sohrmann, D. P. Welchman, P. Zipperlen, and J. Ahringer.

2003. Systematic functional analysis of the *Caenorhabditis elegans* genome using RNAi. Nature 421:231-237.
31. Decker, M., S. Jaensch, A. Pozniakovsky, A. Zinke, K. F. O'Connell, W. Zachariae, E. Myers, and A. A. Hyman. 2011. Limiting amounts of centrosome material set centrosome size in *C. elegans* embryos. Curr Biol 21:1259-1267.
32. Riddle, D. L. 1997. *C. elegans* II. Cold Spring Harbor Laboratory Press, Plainview, N.Y.
33. Tinevez, J. Y., J. Dragavon, L. Baba-Aissa, P. Roux, E. Perret, A. Canivet, V. Galy, and S. Shorte. 2012. A quantitative method for measuring phototoxicity of a live cell imaging microscope. Methods in Enzymology 506:291-309.
34. Pecreaux, J., S. Redemann, Z. Alayan, B. Mercat, S. Pastezeur, C. Garzon-Coral, A. A. Hyman, and J. Howard. 2016. The mitotic spindle in the one-cell *C. elegans* embryo is positioned with high precision and stability. Biophys J 111:1773-1784.
35. Roul, J., J. Pecreaux, and M. Tramier. 2015. Method for controlling a plurality of functional modules including a multi-wavelength imaging device, and corresponding control system. E. P. Office WO2015144650 A1.
36. Kalman, R. E. 1960. A new approach to linear filtering and prediction problems. Journal of Basic Engineering 82:35-45.
37. Jaqaman, K., D. Loerke, M. Mettlen, H. Kuwata, S. Grinstein, S. L. Schmid, and G. Danuser. 2008. Robust single-particle tracking in live-cell time-lapse sequences. Nat Methods 5:695-702.
38. Pecreaux, J., C. Zimmer, and J. C. Olivo-Marin. 2006. Biophysical active contours for cell tracking I: Tension and bending. In Ieee International Conference on Image Processing (Icip), October 8-11 2006, Atlanta, GA, USA. 1949-1952.
39. Hosea, M. E., and L. F. Shampine. 1996. Analysis and implementation of TR-BDF2. Applied Numerical Mathematics 20:21-37.
40. Dogterom, M., and B. Yurke. 1998. Microtubule dynamics and the positioning of microtubule organizing centers. Physical Review Letters 81:485-488.
41. Dogterom, M., J. W. Kerssemakers, G. Romet-Lemonne, and M. E. Janson. 2005. Force generation by dynamic microtubules. Curr Opin Cell Biol 17:67-74.
42. Minc, N., D. Burgess, and F. Chang. 2011. Influence of cell geometry on division-plane positioning. Cell 144:414-426.
43. Mitchison, T., and M. Kirschner. 1984. Dynamic instability of microtubule growth. Nature 312:237-242.
44. O'Rourke, S. M., S. N. Christensen, and B. Bowerman. 2010. Caenorhabditis elegans EFA-6 limits microtubule growth at the cell cortex. Nat Cell Biol 12:1235-1241.
45. O'Toole, E. T., K. L. McDonald, J. Mantler, J. R. McIntosh, A. A. Hyman, and T. Muller-Reichert. 2003. Morphologically distinct microtubule ends in the mitotic centrosome of *Caenorhabditis elegans*. J Cell Biol 163:451-456.
46. Labbe, J. C., E. K. McCarthy, and B. Goldstein. 2004. The forces that position a mitotic spindle asymmetrically are tethered until after the time of spindle assembly. J Cell Biol 167:245-256.
47. Koonce, M. P., and I. Tikhonenko. 2012. Dynein Motor Mechanisms. In Dyneins : structure, biology and disease. S. M. King, editor. Academic Press, Amsterdam ; Boston. xv, 639 p.
48. Wu, J. C., and L. S. Rose. 2007. PAR-3 and PAR-1 inhibit LET-99 localization to generate a cortical band important for spindle positioning in *Caenorhabditis elegans* embryos. Mol Biol Cell 18:4470-4482.

49. Moore, J. K., V. Magidson, A. Khodjakov, and J. A. Cooper. 2009. The spindle position checkpoint requires positional feedback from cytoplasmic microtubules. Current Biology 19:2026-2030.
50. Tanimoto, H., A. Kimura, and N. Minc. 2016. Shape-motion relationships of centering microtubule asters. J Cell Biol 212:777-787.
51. Thery, M., A. Jimenez-Dalmaroni, V. Racine, M. Bornens, and F. Julicher. 2007. Experimental and theoretical study of mitotic spindle orientation. Nature 447:493-496.
52. Farhadifar, R., J. M. Ponciano, E. C. Andersen, D. J. Needleman, and C. F. Baer. 2016. Mutation is a sufficient and robust predictor of genetic variation for mitotic spindle traits in *Caenorhabditis elegans*. Genetics 203:1859-1870.
53. Kimura, K., and A. Kimura. 2011. A novel mechanism of microtubule length-dependent force to pull centrosomes toward the cell center. Bioarchitecture 1:74-79.
54. Grill, S. W., P. Gonczy, E. H. Stelzer, and A. A. Hyman. 2001. Polarity controls forces governing asymmetric spindle positioning in the *Caenorhabditis elegans* embryo. Nature 409:630-633.
55. Kimura, A., and S. Onami. 2007. Local cortical pulling-force repression switches centrosomal centration and posterior displacement in *C. elegans*. J Cell Biol 179:1347-1354.
56. Grill, S. W., and A. A. Hyman. 2005. Spindle positioning by cortical pulling forces. Dev Cell 8:461-465.
57. Labbe, J. C., P. S. Maddox, E. D. Salmon, and B. Goldstein. 2003. PAR proteins regulate microtubule dynamics at the cell cortex in *C. elegans*. Curr Biol 13:707-714.
58. Gusnowski, E. M., and M. Srayko. 2011. Visualization of dynein-dependent microtubule gliding at the cell cortex: implications for spindle positioning. Journal of Cell Biology 194:377-386.
59. Coffman, V. C., M. B. McDermott, B. Shtylla, and A. T. Dawes. 2016. Stronger net posterior cortical forces and asymmetric microtubule arrays produce simultaneous centration and rotation of the pronuclear complex in the early *Caenorhabditis elegans* embryo. Mol Biol Cell 27:3550-3562.
60. Tsou, M. F., A. Hayashi, and L. S. Rose. 2003. LET-99 opposes Galpha/GPR signaling to generate asymmetry for spindle positioning in response to PAR and MES-1/SRC-1 signaling. Development 130:5717-5730.
61. Bringmann, H., C. R. Cowan, J. Kong, and A. A. Hyman. 2007. LET-99, GOA-1/GPA-16, and GPR-1/2 are required for aster-positioned cytokinesis. Curr Biol 17:185-191.
62. Lewellyn, L., J. Dumont, A. Desai, and K. Oegema. 2010. Analyzing the effects of delaying aster separation on furrow formation during cytokinesis in the *Caenorhabditis elegans* embryo. Mol Biol Cell 21:50-62.
63. Wuhr, M., S. Dumont, A. C. Groen, D. J. Needleman, and T. J. Mitchison. 2009. How does a millimeter-sized cell find its center? Cell Cycle 8:1115-1121.
64. Daga, R. R., and P. Nurse. 2008. Interphase microtubule bundles use global cell shape to guide spindle alignment in fission yeast. J Cell Sci 121:1973-1980.
65. Thery, M. 2010. Micropatterning as a tool to decipher cell morphogenesis and functions. J Cell Sci 123:4201-4213.
66. McIntosh, J. R., M. I. Molodtsov, and F. I. Ataullakhanov. 2012. Biophysics of mitosis. Quarterly reviews of biophysics 45:147-207.
67. Musacchio, A. 2011. Spindle assembly checkpoint: the third decade. Philosophical transactions of the Royal Society of London. Series B, Biological sciences 366:3595-3604.

68. Garzon-Coral, C., H. A. Fantana, and J. Howard. 2016. A force-generating machinery maintains the spindle at the cell center during mitosis. Science 352:1124-1127.
69. Redemann, S., J. Baumgart, N. Lindow, M. Shelley, E. Nazockdast, A. Kratz, S. Prohaska, J. Brugues, S. Furthauer, and T. Muller-Reichert. 2017. *C. elegans* chromosomes connect to centrosomes by anchoring into the spindle network. Nat Commun 8:15288.
70. Maton, G., F. Edwards, B. Lacroix, M. Stefanutti, K. Laband, T. Lieury, T. Kim, J. Espeut, J. C. Canman, and J. Dumont. 2015. Kinetochore components are required for central spindle assembly. Nat Cell Biol 17:697-705.
71. Gierke, S., P. Kumar, and T. Wittmann. 2010. Analysis of microtubule polymerization dynamics in live cells. Methods in cell biology 97:15-33.
72. Laan, L., N. Pavin, J. Husson, G. Romet-Lemonne, M. van Duijn, M. P. Lopez, R. D. Vale, F. Julicher, S. L. Reck-Peterson, and M. Dogterom. 2012. Cortical dynein controls microtubule dynamics to generate pulling forces that position microtubule asters. Cell 148:502-514.
73. Olson, S. K., G. Greenan, A. Desai, T. Muller-Reichert, and K. Oegema. 2012. Hierarchical assembly of the eggshell and permeability barrier in *C. elegans*. J Cell Biol 198:731-748.
74. Costantino, S., J. W. Comeau, D. L. Kolin, and P. W. Wiseman. 2005. Accuracy and dynamic range of spatial image correlation and cross-correlation spectroscopy. Biophys J 89:1251-1260.
75. Ahringer, J. 2003. Control of cell polarity and mitotic spindle positioning in animal cells. Current Opinion in Cell Biology 15:73-81.
76. Edwards, J. 1892. An elementary treatise on the differential calculus, with applications and numerous examples. Macmillan, London, New York,.
77. Farhadifar, R., C. F. Baer, A. C. Valfort, E. C. Andersen, T. Muller-Reichert, M. Delattre, and D. J. Needleman. 2015. Scaling, selection, and evolutionary dynamics of the mitotic spindle. Curr Biol 25:732-740.
78. Freeman, D. L., and D. J. D. 1983. The influence of diffusion on surface reaction kinetics. The Journal of Chemical Physics 78:6002.
79. Freeman, D. L., and J. D. Doll. 1983. Langevin analysis of the diffusion model for surface chemical reactions. The Journal of Chemical Physics 79:2343.
80. Goehring, N. W., C. Hoege, S. W. Grill, and A. A. Hyman. 2011. PAR proteins diffuse freely across the anterior-posterior boundary in polarized *C. elegans* embryos. J Cell Biol 193:583-594.
81. Erickson, H. P. 2009. Size and shape of protein molecules at the nanometer level determined by sedimentation, gel filtration, and electron microscopy. Biol Proced Online 11:32-51.
82. Adam, G., and M. Delbruck. 1968. Reduction of dimensionality in biological diffusion processes. In Structural Chemistry and Molecular Biology. A. Rich, N. R. Davidson, and L. Pauling, editors. W. H. Freeman, San Francisco. 198-215.
83. Nadrowski, B., P. Martin, and F. Julicher. 2004. Active hair-bundle motility harnesses noise to operate near an optimum of mechanosensitivity. Proc Natl Acad Sci U S A 101:12195-12200.
84. Mercat, B., X. Pinson, J. Fouchard, H. Mary, S. Pastezeur, Z. Alayan, Y. Gachet, S. Tournier, H. Bouvrais, and J. Pécréaux. 2016. Spindle micro-fluctuations of length reveal its dynamics over cell division. Biophysical Society meeting, Los Angeles (CA), USA. In Biophys J 110:622a.

TABLES

Characteristic measured (mean ± SD)	**control #1 (*N* = 10)**	***such-1(h1960)* (*N* = 13)**	**control #2 (*N* = 10)**	***spd-2(RNAi)* (*N* = 12)**
Oscillation onset *T1* (s)	-9.54 ± 8.04	-80.56 ± 37 $p = 1 \times 10^{-5}$	-5.14 ± 20.19	9.49 ± 17.44 $p = 0.043$
Posterior centrosome (CS) reaching 70% of the AP axis *T2* (s)	-9.19 ± 8.42	-89.78 ± 45.10 $p = 3 \times 10^{-5}$	-5.24 ± 21.18	-0.53 ± 14.81 $p = 0.43$
Maximum oscillation amplitude (posterior) (%)	23.90 ± 3.39	21.88 ± 3.56 $p = 0.18$	16.10 ± 3.45	14.64 ± 4.73 $p = 0.39$
Nuclear envelope breakdown time (s)	- 150.1 ± 31.2	- 284.9 ± 38.7 $p = 2 \times 10^{-8}$	-194.83 ± 26.60	-170.0 ± 15.51 $p = 0.04$
Oscillation die down *T3* (s)	114.90 ± 22.63	109.69 ± 16.23 $p = 0.55$	111.50 ± 15.52	114.4 ± 23.8 $p = 0.74$
Oscillation duration *T3* - *T1* (s)	124.44 ± 18.93	190.25 ± 30.13 $p = 3 \times 10^{-6}$	116.64 ± 20.01	104.9 ± 18.9 $p = 0.096$
Posterior centrosome position at oscillation onset (%)	70.03 ± 1.73	70.48 ± 1.85 $p = 0.56$	70.12 ± 1.23	72.46 ± 1.76 $p = 0.0016$
Posterior centrosome position at oscillation die down (%)	80.31 ± 2.04	80.72 ± 1.99 $p = 0.63$	79.69 ± 1.94	81.46 ± 1.33 $p = 0.025$
Embryo length (µm)	49.23 ± 2.34	47.26 ± 3.34 $p = 0.11$	50.33 ± 3.18	51.08 ± 2.78 $p = 0.56$
Embryo width (µm)	33.10 ± 2.36	31.85 ± 1.94 $p = 0.19$	30.60 ± 1.80	30.49 ± 1.56 $p = 0.88$

Table 1: Timing and position of metaphase and anaphase events in delayed-anaphase mutants and in reduced-microtubule-nucleation embryos. Embryos with labeled centrosomes were imaged at 23°C and spindle poles tracked. We first compared labeled SPD-2^{CEP192}::GFP;mCherry::HIS-58^{H2B} embryos with (*N* = 13) and without (*N* = 10) non-null mutation *such-1*^{ANAPC5}*(h1960)*. This gene codes for an APC/C component (29). We also compared embryos whose centrosomes were labeled using GFP::γ-tubulin, and which were treated with *spd-2(RNAi)* (*N* = 12) or L4440 empty vector (*N* = 10). Times were measured from the onset of anaphase, determined from the onset of spindle elongation (34). Peak-to-peak oscillation amplitude is shown as a percentage of embryo width. Positions along the AP axis are shown as a percentage of embryo length. Error bars indicate standard deviations. *p* values are reported for Student's *t*-test, Welch-Satterthwaite corrected. Succession of the key timing events, i.e. NEBD, *T*1, *T*2 and *T*3, are schematized in Fig. S4D and explained in Methods.

FIGURE LEGENDS

Figure 1: Microtubule contact density at the cell cortex.
(**A-C**) Exemplar spinning disk micrographs of *Caenorhabditis elegans* at the cortical plane with YFP::α-tubulin labeling of microtubules (MTs), viewed at 10 frames per second. Posterior tip of the embryo is on the right side of the pictures. The raw image (A) was de-noised (B) using the Kalman filter and microtubule contacts tracked (C, green lines) using u-track algorithm with the parameters listed in Methods. Scale bars represent 10 μm. (**D**) Experimental setup for viewing microtubule contact density at the cell cortex. The scale represents the 10 regions along the anteroposterior (AP) axis used for analysis (Methods). Red and blue disks represent the anterior and posterior centrosomes, respectively, and the light blue clouds are the chromosomes. Microtubules emanating from the centrosomes are exemplified using thin black lines. The posterior-most crescent where the active force generators are located (so-called the active region) corresponds to the purple cortical region. (**E**) Semi-log plot of the histogram of the microtubule contact durations at the cortex during metaphase and anaphase for a single embryo (black dots), fitted with an exponential decay (grey line) corresponding to a characteristic time of 0.95 ± 0.03 s (*N* = 3832 microtubule contacts). (**F-G**) Microtubule contact densities at the cortex obtained by analyzing spinning disk microscopy images of (F) the YFP::α-tubulin-labeled microtubule strain in *N* = 12 *C. elegans* embryos and (G) the GFP::β-tubulin-labeled microtubule strain in *N* = 8 *Caenorhabditis briggsae* embryos. Microtubule contact densities measured at 23°C for each embryo were then averaged along the AP axis within 10 regions of equal width and over a 10-second running time window, and finally the average over embryos was computed (Methods).

Figure 2: Astral microtubules preferentially contact the cortex in the area closest to the centrosomes.
(**A**) Microtubule (MT) contact density at the cell cortex in *Caenorhabditis elegans* with superposed centrosome trajectories obtained by combining two data sets. First, the densities, shown here as an interpolated heat map, were measured in the microtubule-labeled strain at the cortex and obtained by averaging the densities along the anteroposterior (AP) axis within 10 regions of equal width and over a 10-second running time window, finally taking the mean over embryos (Methods). Data are the same as in Fig. 1F. Second, the average trajectories of the centrosomes were obtained by imaging the same strain at the spindle plane (*N* = 8 embryos) and superposed on the microtubule contact density map. The dashed line represents the anterior centrosome trajectory, and the solid line indicates the posterior one. At the bottom, a schematic of the experimental setup where centrosomes are shown as black disks, with thin black lines depicting the astral microtubules. Microtubule contacts at the cortex are shown as green dots. The active region, which is used to compute panel C, corresponds to the purple cortical horizontal line. (**B**) Modeled number of microtubules contacting the cortex in the active region versus the posterior displacement of the centrosome along the AP axis, with the active region boundary expressed as a percentage of embryo length. The thick black line corresponds to a boundary at 70%, mimicking the untreated embryo. In this case, the number of contacts started to increase steeply at a position above 60% (purple line). Blue and green curves model *let-99(RNAi)* or *par-3(RNAi)* experiments where the boundary was displaced anteriorly. Red and orange curves show the cases of posteriorly displaced boundaries. (**C**) Density of microtubule contacts versus the position of the posterior centrosome in a region ranging from 70% to 100% of the AP axis, computed from the data shown in panel A. (**D**) Microtubule contact density at the cortex in *C. briggsae* with superposed centrosome trajectories represented similarly to panel A. Microtubule contact densities at the cortex were obtained by viewing a GFP::β-tubulin-labeled microtubule strain. The data are the same as in Fig. 1G. Centrosome trajectories were obtained in a second experiment by imaging a GFP::γ-tubulin;GFP::HIS-11-labeled centrosome and histone strain (*N* = 7 *C. briggsae* embryos) at the spindle plane.

Figure 3: Expanded model accounts for positional and temporal regulations of cortical forces.

(**A**) Schematics of the expanded model, highlighting the players (top row), the quantity they regulate (second row), how they control forces (module, third row) and some related phenotypes (bottom row). Pink/yellow colors correspond to the positional control, involving astral microtubule dynamics and the active region created by LET-99, and blue depicts the time control, involving force generator dynamics. While both controls participate to oscillation onset (purple), final spindle position mostly depends on active region extent (yellow) and oscillation die down on time control (blue). (**B**) Modeled number of engaged force generators versus the posterior displacement of the centrosome along the anteroposterior (AP) axis, with the active region boundary expressed as a percentage of embryo length. The thick black line represents the case in which active region boundary is located at 70% of the AP axis, mimicking the control embryo. Blue and green curves model *let-99(RNAi)* and *par-3(RNAi)* experiments where the boundary was displaced anteriorly. Red and orange curves show cases of posteriorly displaced boundaries. Grey shading indicates when the number of engaged force generators is too low to permit oscillation. The parameters used are listed in Table S5. (**C-D**) Positions of the posterior centrosome at oscillation onset (C) in *let-99(RNAi)* (N = 15) and control (N = 12) embryos and (D) in *par-3(RNAi)* (N = 19) and control (N = 17) embryos, with centrosomes labeled by GFP::γ-tubulin. Bee swarm plots report values obtained for each embryo. Large thick horizontal bars depict the mean while error bars indicate SD and asterisks indicate significant differences (Methods).

Figure 4: Embryo length has less effect on oscillation onset position than on its timing.
(**A**) Modeled number of engaged force generators versus the posterior displacement of the centrosome along the AP axis as a percentage of embryo length. The line colors indicate the embryo length: untreated embryos are black; the shorter embryos corresponding to those produced by *cid-1(RNAi)*, *ima-3(RNAi)* or *ani-2(RNAi)* are shown in blue and green*;* and the longer embryos from *c27d9.1(RNAi)* are shown in red and orange. The parameters used are listed in Table S5. Grey shading indicates when the number of engaged force generators was too low to permit oscillation. (**B**) Embryo lengths in control embryos and those treated by *RNAi* to vary their lengths. Error bars indicate SD, and asterisks indicate significant differences (Methods). (**C**) Shift in the posterior centrosome position at oscillation onset as compared to the control (normalized by the average embryo length in control, see Methods) and (**D**) shift in oscillation onset timing normalized by the control's average pro-metaphase and metaphase duration, both versus the variations in embryo lengths as compared to the control. The solid black lines indicate the linear least square fits, with slopes of -0.09 ± 0.03 (p = 8 x 10^{-4} compared to null slope) and 0.51 ± 0.06 (p = 1 x 10^{-11}), respectively. We measured N = 9 *cid-1(RNAi)*, N = 6 *c27d9.1(RNAi), N* = 12 *ani-2(RNAi)*, N = 6 *ima-3(RNAi)* and N = 49 control embryos with GFP::γ-tubulin-labeled centrosomes. The dashed black lines are the standard errors. Dots indicate individual embryos, and the average control values (0 shift) are thin black lines.

Figure 5: Two independent controls both contribute to oscillations.
(**A**) Stability diagram of the full-expanded model as a function of the detachment rate (off-rate $\overline{k_{off}}$, inverse of the processivity, x-axis) and of the position of the centrosome as a percentage of embryo length (y-axis). The unstable region (blue) corresponds to the values of off-rate and posterior-centrosomal position enabling oscillation development. The critical values are marked by the thick blue and green lines for parameters corresponding to control condition. Thin blue lines with various dashing patterns correspond to oscillation onset's critical curves for parameters distinct from the control, indicated by their raw values and their relative values in % of control condition, and corresponding to experimental perturbations. The orange arrow indicates the typical "phase" trajectory during mitosis, based on the parameters used in this study. The greyed-out area depicts that above a detachment rate threshold, the posterior displacement of the spindle/posterior centrosome no longer occurs (orange curve in Fig. 6G). The centrosome needs to reach a position that is posterior enough to enable oscillations, while force generators must display a high enough processivity (measured to 1-2 s^{-1} in metaphase (14)). The parameters used are listed in Table S5. (**B-D**) Timings of oscillation onset, oscillation die down and posterior centrosome arrival at 70% of embryo length (B-C) when the size of the active region is changed in *let-99(RNAi)* (N = 15) compared to control (N = 12) embryos or in *par-3(RNAi)* (N = 19) compared to control (N = 17) embryos, and (D) upon depletion of active force

generators (f.g.) in *gpr-1/2(RNAi)* (*N* = 19) compared to *N* = 10 control embryos. All embryos display GFP::γ-tubulin labeling of the centrosomes. Bee swarm plots report values obtained for each embryo. Large thick horizontal bars depict the mean while error bars indicate SD and asterisks indicate significant differences (Methods).

Figure 6: Active region boundary position sets the final spindle position.
(**A-C**) Posterior centrosome position at oscillation die down (AB) upon anteriorly extending the active region (A) by *let-99(RNAi)* (*N* = 15 embryos) compared to control (*N* = 12 embryos) or (B) by *par-3(RNAi)* (*N* = 19) compared to control (*N* = 17), and (C) upon decreasing cortical force generation by *gpr-1/2(RNAi)* (*N* = 19) compared to *N* = 10 control embryos. In all cases, centrosomes were labeled by GFP::γ-tubulin. Bee swarm plots report values obtained for each embryo. Large thick horizontal bars depict the mean while error bars indicate SD and asterisks indicate significant differences (Methods). (**D-H**) Posterior displacement of the posterior centrosome averaged over 25 simulation runs with parameters varied as follows: (D) the position of the boundary of the active region; (E) the binding rate (on-rate) of the force generators to the microtubules $\widehat{k_{on}}$, whose asymmetry may encode the polarity (14); (F) the total number of active force generators available at the posterior active region *N* (active, i.e. currently pulling or ready to do so when meeting a microtubule); (G) the force generator (f.g.) final detachment rate (off-rate, the inverse of the processivity) $\overline{k_{off}^{\infty}}$; and (H) the number of microtubules emanating from each centrosome (in % of control, which has *M* = 3000 MTs per centrosome). When it does not depend on the parameter considered, the initial model is shown by a dashed grey line. In all cases, the control values are black; lower values are blue and green; and the higher values are red and orange. The dispersions of the final values for each case are represented on the right side of the plots by purple arrows in dashed or solid lines according to the model used. There, a large span reveals a lack of robustness to parameter variations, while a circle is used when the parameter has no effect on the final value.

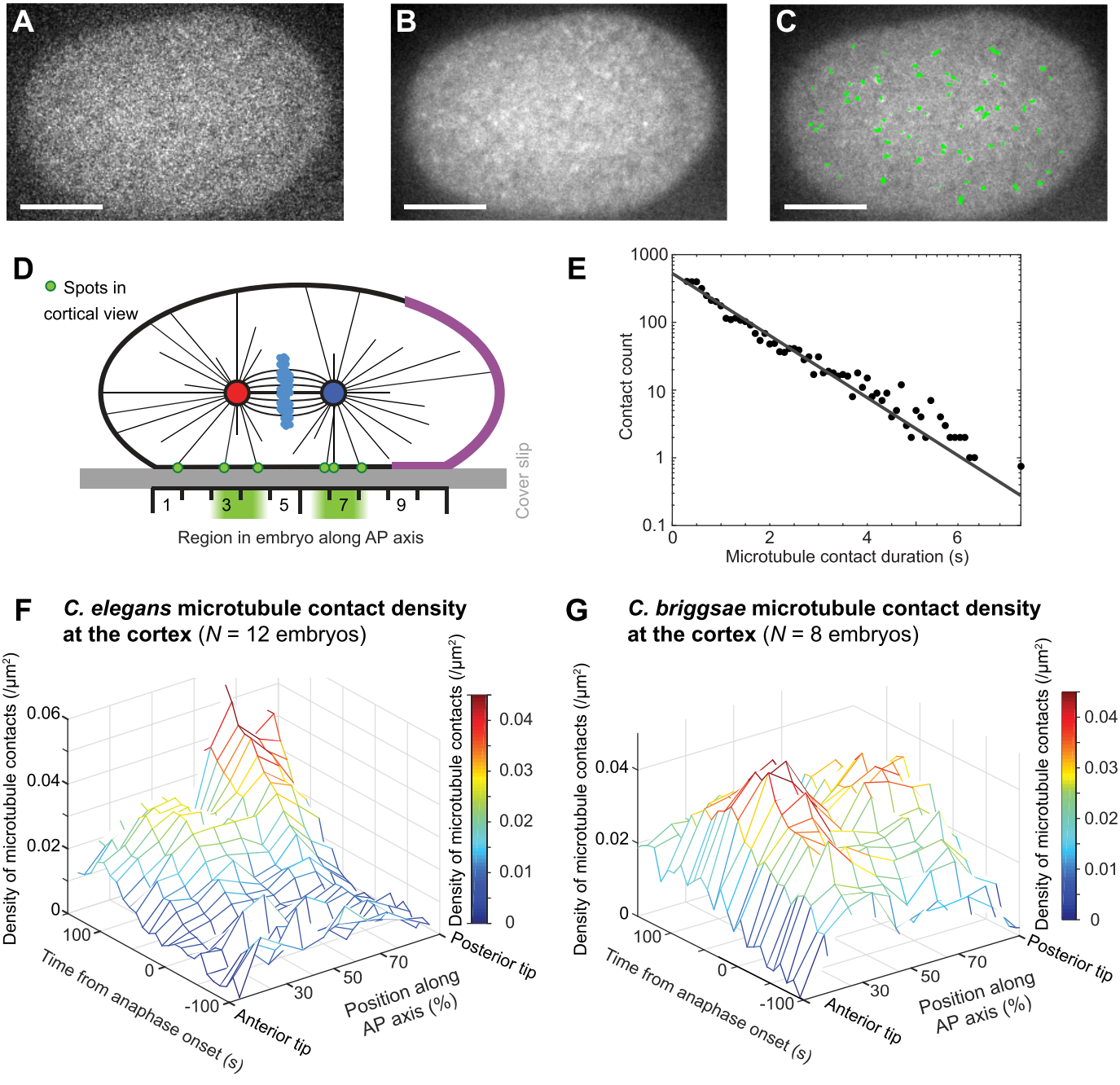
A
B
C
D
Spots in cortical view
1
3
5
7
9
Cover slip
Region in embryo along AP axis
E
Contact count
Microtubule contact duration (s)
F
C. elegans microtubule contact density at the cortex (N = 12 embryos)
Density of microtubule contacts (/μm²)
Time from anaphase onset (s)
Anterior tip
Position along AP axis (%)
Posterior tip
G
C. briggsae microtubule contact density at the cortex (N = 8 embryos)

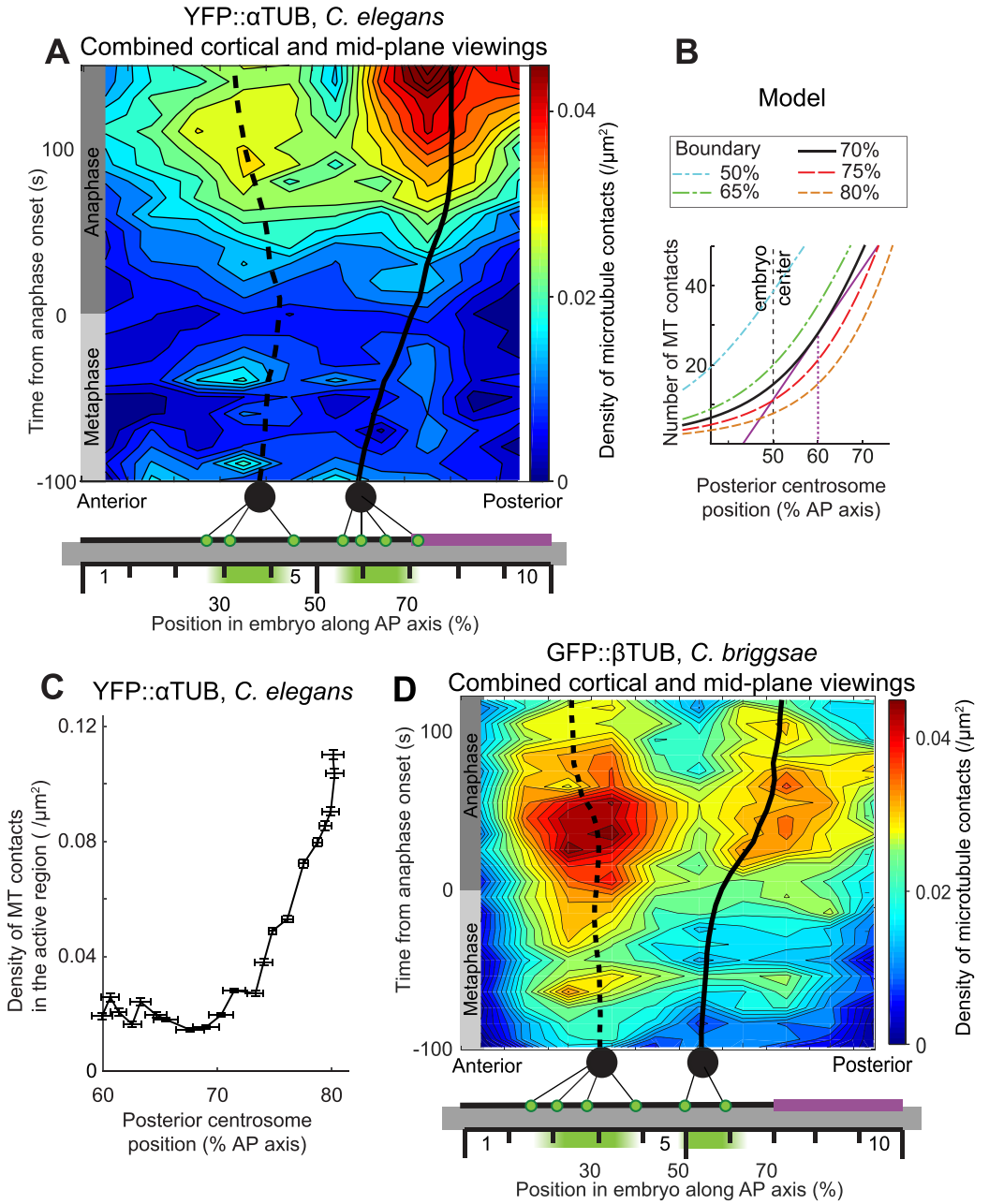
YFP::αTUB, C. elegans
A
Combined cortical and mid-plane viewings
Anaphase
Metaphase
Time from anaphase onset (s)
100
0
-100
0.04
0.02
0
Density of microtubule contacts (/μm²)
Anterior
Posterior
1
5
10
30
50
70
Position in embryo along AP axis (%)
B
Model
Boundary
50%
65%
70%
75%
80%
embryo center
Number of MT contacts
40
20
50
60
70
Posterior centrosome position (% AP axis)
C
YFP::αTUB, C. elegans
Density of MT contacts in the active region (/μm²)
0.12
0.08
0.04
0
60
70
80
Posterior centrosome position (% AP axis)
GFP::βTUB, C. briggsae
D
Combined cortical and mid-plane viewings
Anaphase
Metaphase
Time from anaphase onset (s)
100
0
-100
0.04
0.02
0
Density of microtubule contacts (/μm²)
Anterior
Posterior
1
5
10
30
50
70
Position in embryo along AP axis (%)

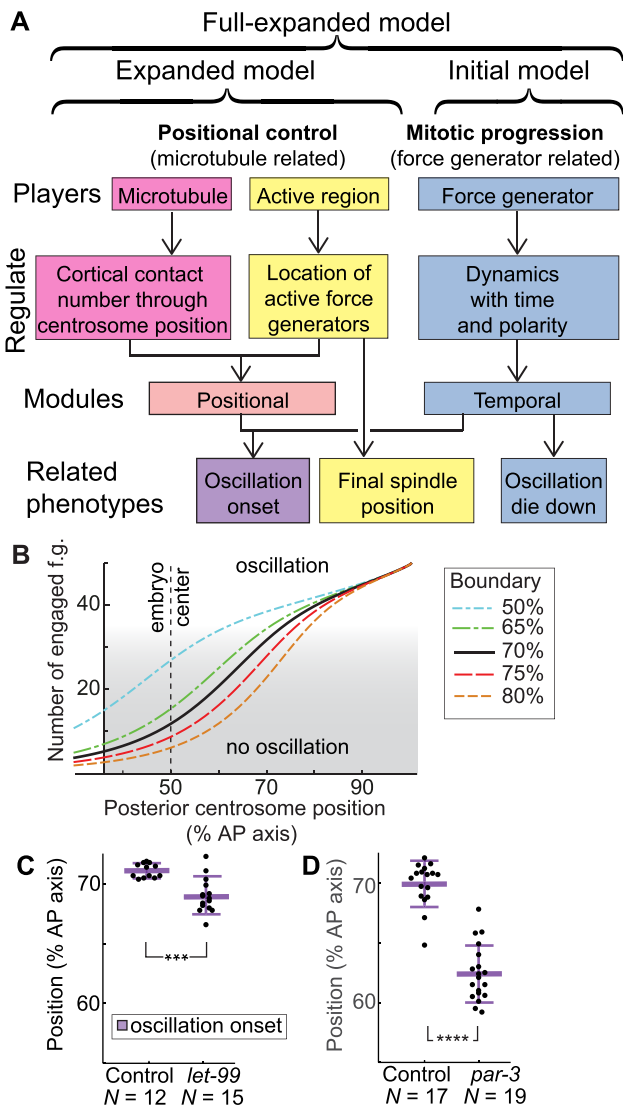
A
Full-expanded model
Expanded model
Initial model
Positional control
(microtubule related)
Mitotic progression
(force generator related)
Players
Microtubule
Active region
Force generator
Regulate
Cortical contact number through centrosome position
Location of active force generators
Dynamics with time and polarity
Modules
Positional
Temporal
Related phenotypes
Oscillation onset
Final spindle position
Oscillation die down
B
Number of engaged f.g.
embryo center
oscillation
no oscillation
Boundary
50%
65%
70%
75%
80%
Posterior centrosome position
(% AP axis)
C
Position (% AP axis)
***
oscillation onset
Control
N = 12
let-99
N = 15
D
Position (% AP axis)
****
Control
N = 17
par-3
N = 19

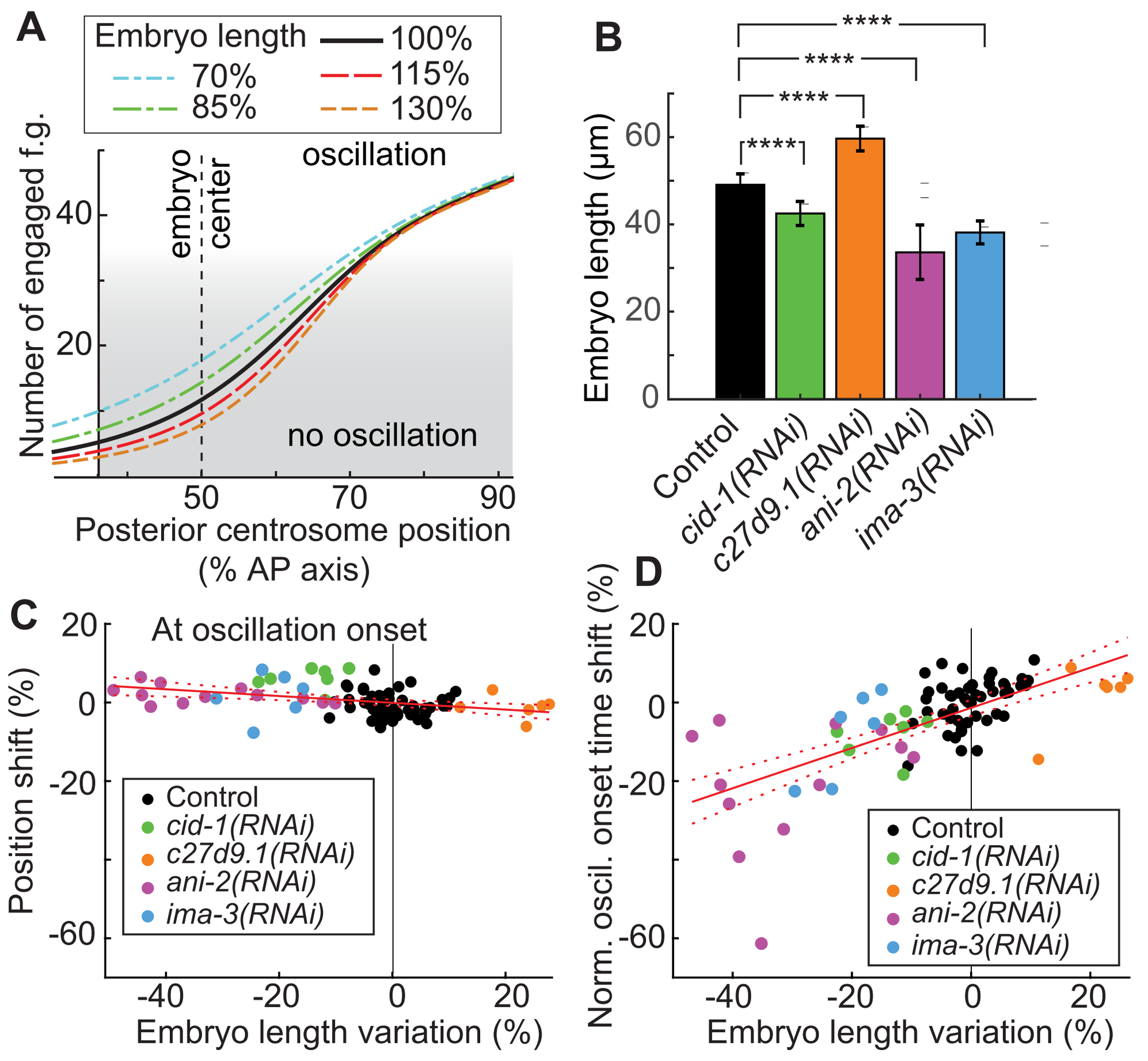
A
Embryo length
100%
70%
115%
85%
130%
oscillation
embryo center
no oscillation
Number of engaged f.g.
40
20
50
70
90
Posterior centrosome position
(% AP axis)
B
****
****
****
****
Embryo length (µm)
60
40
20
0
Control
cid-1(RNAi)
c27d9.1(RNAi)
ani-2(RNAi)
ima-3(RNAi)
C
At oscillation onset
Position shift (%)
20
0
-20
-60
Control
cid-1(RNAi)
c27d9.1(RNAi)
ani-2(RNAi)
ima-3(RNAi)
-40
-20
0
20
Embryo length variation (%)
D
Norm. oscil. onset time shift (%)
20
0
-20
-60
Control
cid-1(RNAi)
c27d9.1(RNAi)
ani-2(RNAi)
ima-3(RNAi)
-40
-20
0
20
Embryo length variation (%)

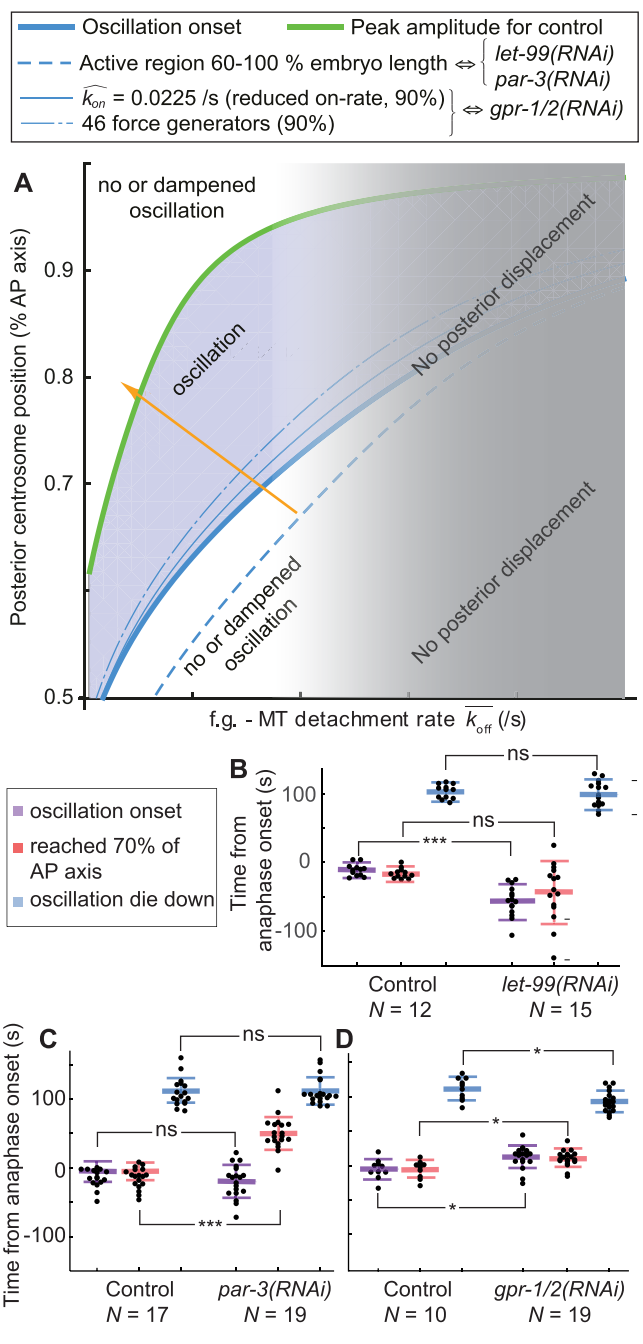
Oscillation onset
Peak amplitude for control
Active region 60-100 % embryo length ⇔ let-99(RNAi) par-3(RNAi)
$\widehat{k_{on}}$ = 0.0225 /s (reduced on-rate, 90%)
46 force generators (90%) ⇔ gpr-1/2(RNAi)
A
no or dampened oscillation
oscillation
No posterior displacement
No posterior displacement
no or dampened oscillation
Posterior centrosome position (% AP axis)
0.9
0.8
0.7
0.5
f.g. - MT detachment rate $\overline{k_{off}}$ (/s)
oscillation onset
reached 70% of AP axis
oscillation die down
B
Time from anaphase onset (s)
100
0
-100
ns
ns
***
Control
N = 12
let-99(RNAi)
N = 15
C
Time from anaphase onset (s)
100
0
-100
ns
ns
***
Control
N = 17
par-3(RNAi)
N = 19
D
*
*
*
Control
N = 10
gpr-1/2(RNAi)
N = 19

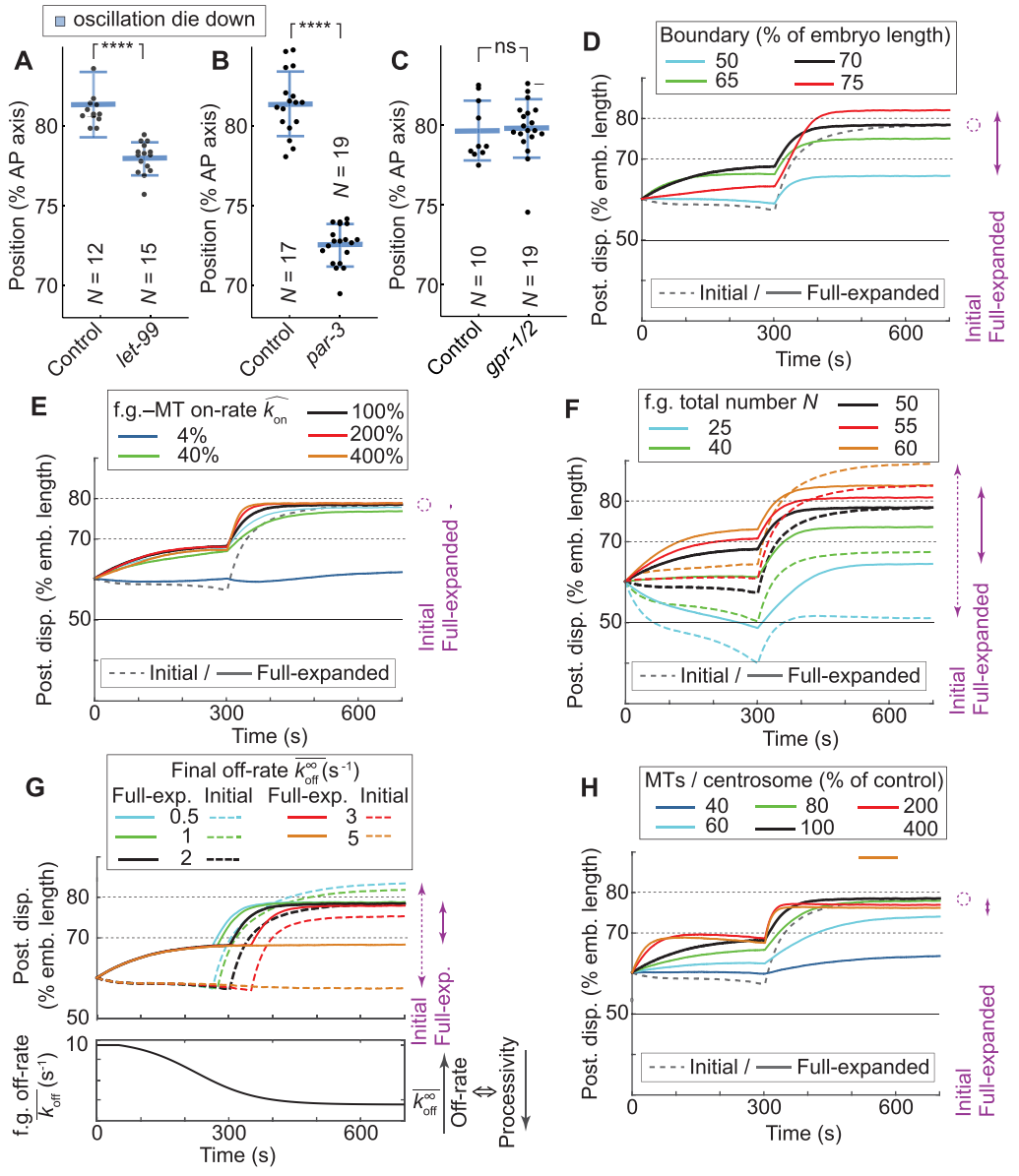
oscillation die down
A
B
C
D
E
F
G
H
Position (% AP axis)
N = 12
N = 15
N = 17
N = 19
N = 10
N = 19
Control
let-99
par-3
gpr-1/2
****
ns
Boundary (% of embryo length)
50
65
70
75
Post. disp. (% emb. length)
Time (s)
Initial / Full-expanded
Initial
Full-expanded
f.g.–MT on-rate $\widehat{k_{on}}$
4%
40%
100%
200%
400%
f.g. total number N
25
40
50
55
60
Final off-rate $\overline{k_{off}^{\infty}}$ (s^{-1})
Full-exp.
Initial
0.5
1
2
3
5
Post. disp. (% emb. length)
Initial
Full-exp.
f.g. off-rate $\overline{k_{off}}$ (s^{-1})
$\overline{k_{off}^{\infty}}$
Off-rate
Processivity
MTs / centrosome (% of control)
40
60
80
100
200
400